New approaches to field-model data comparison: Numerical modelling of the last glacial cycle in the Welland catchment, England

Briant, R.M.[a*], Wainwright, J.[b], Maddy, D.[c]

[a]Department of Geography, Birkbeck, University of London, Malet Street, London, WC1E 7HX, UK

[b]Department of Geography, Durham University, Science Laboratories, South Road, Durham, DH1 3LE, UK

[b] School of Geography, Politics and Sociology, Newcastle University, Newcastle upon Tyne, NE1 7RU, UK

*Corresponding author: Tel: +44 (0)20 3073 8444; Email: b.briant@bbk.ac.uk

Abstract

The extent to which deposition within river systems is driven by climate over glacial-interglacial timescales, and the nature of such linkages, is much debated. Answering such questions from the geological record is often limited by a lack of geochronological precision. Numerical modelling allows us to scale up what we know of climate response on short timescales to these longer timescales. To generate a robust reconstruction, relevant parameters need to be included in the model setup, and model output needs to be evaluated against the geological record. Here we introduce the model CLEOPATRA (CybErosion-based Landscape Evolution On Periglacially Altered TeRrAin), the first reduced complexity model to include periglacial processes explicitly within a river catchment. We also use a pattern-oriented sampling approach to model evaluation and introduce innovative methods, particularly the quantification of the comparison of synthetic borehole data with geological sequences using Spearman rank correlation. Sediment starvation is observed within the model compared with the geological data, suggesting either the importance of sediment reworking within the catchment or that we have yet to specify the full complexity of periglacial processes in the model. In this sediment-starved situation, gelifluxion drives sediment supply but climate is less important in dictating the timing of aggradation and incision than intrinsic controls and elapsed time.

Keywords: landscape; modelling; catchment; OSL; radiocarbon; periglacial

1. Introduction

Whilst much basin research has suggested that deposition in fluvial systems is driven by base-level changes, leading to a predictable sequence stratigraphy that can be linked to high and lowstand phases (e.g., Shanley and McCabe, 1994), recent research on Quaternary systems has shown instead the importance of upstream controls (e.g., Blum and Törnqvist, 2000). Broadly, these upstream controls are driven by climate, with the changing balance between stream power and sediment supply driving phases of incision and aggradation. For example, Pratt-Situala et al. (2004) showed how periods of monsoon intensification drove significant aggradation in the Marsyandi River in Nepal. The role of climate in driving characteristics of sedimentary sequences is, however, mediated by multiple local factors, such as angle of adjacent sediment-feeding hillslopes, dominant processes operating, or durability of different lithologies (Attal, 2017).

This complexity means that the relationship between climate and river response is much debated (e.g., Wainwright, 2006; van de Wiel and Coulthard, 2010), with some arguing that in some catchments the sediment flux signal coming out of the source region could be buffered, or even completely 'shredded' with relation to the original signal (e.g., Jerolmack and Paola, 2010; Blöthe and Korup, 2013). In addition, episodic sediment supply and spatial variability may lead to shifts between 'flood depositing' and 'flood cleaning' in different reaches at different times (Turowski et al., 2013), meaning that even a single catchment will be more or less climate sensitive depending on recent history. In addition to catchment complexity, this debate is also partly because geological records lack the chronological resolution to trace leads and lags in the system. In contrast, assessment of the timing of the relationships between external factors and internal responses to them should be possible using numerical modeling of landscape evolution in more detail. This will enable clearer separation between the influence of intrinsic and extrinsic drivers in any one catchment (Veldkamp et al., 2017). This modelling work, however, needs to be grounded in evaluation against real-world data sets, as long as such field data sets are collected appropriately (Briant et al., 2018). Such evaluation, if successful, increases the plausibility

of narratives gained from numerical models that explain the suites of geomorphological features developed in a catchment over geological timescales.

Many landscape-evolution models are however applied to abstract landscapes (Temme et al., 2017; Veldkamp et al., 2017), owing to 'difficulties in determining initial conditions and validating the model results' (van de Wiel et al., 2011, p. 175). Evaluating model results is indeed challenging because of to mismatches in the types of data generated. For example, field stratigraphic investigations generate detailed site-specific field data with significant and uncertain time gaps even with the most robust chronologies compared with continuous three-dimensional model data. Also, time-series outputs at the catchment outflow are the simplest output to produce from models but are not regularly available from field data over appropriate timescales. Developing new approaches (e.g., pattern-oriented sampling – Briant et al., 2018) is therefore necessary to compare the two types of data that measure field data and generate model output that are more comparable with each other (e.g., Temme et al., 2017). Furthermore, by providing more spatial and temporal information to evaluate model results, model equifinality can be constrained, if never completely eliminated (e.g., Veldkamp et al., 2017).

The study reported in this paper sought to understand the role of climate in driving fluvial activity by applying numerical modelling to the development of a river catchment over the last glacial / interglacial cycle (ca. 140,000 years). To achieve this we applied innovative approaches to model evaluation. The geological sequences are from a low-lying river catchment in the northern Fenland (eastern England) and contain fossil material providing evidence of local climate change and sedimentological evidence of system change. They are dated using optically stimulated luminescence (OSL) dating on sand grains and radiocarbon dating (Briant, 2002; Briant et al., 2004a, 2004b). The modelling was undertaken using CLEOPATRA (CybErosion-based Landscape Evolution On Periglacially Altered TeRrAin), a spatially distributed reduced-complexity cellular model based on that initially applied over long timescales by Wainwright (2006). Following robust evaluation of model output against geological data using a pattern-oriented sampling approach (Briant et al., 2018), we assess the extent to which climate drives the balance between incision and aggradation in the Welland catchment over the last glacial period, at a much higher temporal resolution than is available when using conceptual models based on field data.

2. Geological background to the study area

The Welland catchment is located in the northern part of the Fenland Basin of eastern England (Fig. 1A) and has a relatively complete geological record of river activity over the last interglacial-glacial cycle (140,000 years). The Fenland Basin is a large, shallow basin formed within Jurassic-aged clays into which a number of river systems drain. At the present day the seaward end of this basin is characterised by large expanses of fen fringed by saltmarsh. During the Last Glacial Maximum it would have been a periglacial plain crossed by several major gravel-bed rivers. The Welland catchment has an area of ca. 1 656 km^2 (Environment Agency, 2009), and a channel length of ca. 105 km. The topography of the catchment is moderate (Fig. 1B), with a maximum basin elevation of just over 200 m and ca. 30% of the downstream area below 10 m OD. The upstream area of the catchment would have been the same at the Last Glacial Maximum. The downstream extension of the catchment was presumably much greater, as sea level dropped by ca. 120 m, moving the local coastline to the western end of the English Channel and leaving the Fenland rivers draining into a delta in the southern North Sea. Despite this, the catchment was not significantly influenced by sea-level changes because of the shallow offshore coastal shelf, making it highly suitable for studying upstream influences on fluvial sedimentation. The exact dimensions of the Welland catchment at the last glacial maximum are unclear as the associated gravel deposits thin in a seaward direction and are absent even at the present-day coastline. Modern mean annual precipitation is 588 mm (Climate Data, 2015), and mean annual discharge is ca. 50 $m^3 s^{-1}$ (Environment Agency, 2012). Mean annual temperature at Market Deeping is 9.8°C (Climate Data, 2015). The catchment is thought to be sensitive to climate changes over the last glacial period because the relatively small drainage basin and low relief decrease complexity of response (e.g., van Huissteden and Kasse, 2001). In addition, the river was believed to be independent of ice-sheet influence because it lies outside the limit of glacial advance during the last glacial period (Hughes et al., 2013). Whilst the catchment lies on the flanks of the slowly subsiding North Sea basin, no other tectonic effects are reported (Duff and Smith, 1992) so tectonic factors were not modelled.

The upper and middle reaches of the Welland are underlain and flanked by mudstones of the Jurassic Lias Group. As the river flows northeastward, rocks of the Inferior and Great Oolite Groups become

dominant, forming a small escarpment and constraining river flow through a valley at Stamford (Fig. 1C). Downstream of Stamford, the river flows over Jurassic Oxford Clay of the Ancholme Group. This changing bedrock geology has a strong control on the Quaternary geology of the catchment, with river-gravel deposits present in greater abundance where the bedrock is less resistant (e.g., at the edge of the Fenland Basin; Fig. 1C). The only significant river deposits in the region are the First Terrace Gravel shown on Fig. 1C, which is defined as a gravel deposit that lies beneath and adjacent to the current floodplain and takes a fan-like shape as the river enters the Fenland (Horton and Downing, 1989). The sequence within this fan is up to 6 m thick (Fig. 2), thins toward the Fenland Basin, and is overlain by Holocene peats and silts. Evidence suggests that deposits within it date from just before the last interglacial (French, 1982; Davey et al., 1991; Keen et al., 1999) to the present day, although fragments of older deposits may also exist (Davey et al., 1991).

The records used to compare with model output in this paper are a composite of those from observations made between 1998 and 2002 (Briant, 2002; Briant et al., 2004a,b) and earlier work describing older deposits (French, 1982; Davey et al., 1991; Keen et al., 1999). Sediments at six different locations in the downstream part of the catchment (Fig. 2, Table 1; Briant, 2002; Briant et al., 2004a, b) show distinct phases of deposition that can be traced across the catchment apparently in response to distinct phases of climate reconstructed from fossil assemblages. Each phase is represented by a dated sedimentary unit that is observed at multiple locations, and five of these nine phases have been dated using radiocarbon and OSL dating. Fig. 2 and Table 1 show that the dating of these phases varies in robustness. In particular, phase 4 has no chronological control, with an age instead inferred in relation to the underlying phase 3 sediments in the southern part of the fan and overlying phase 5 sediments in the northern part. Phase 4, which is unfortunately the most spatially widespread sedimentary unit, is therefore likely to be diachronous with an erosional base that likely spans a considerable period of time. The other phases have much better chronological control, and significant diachroneity seems less likely. At two locations, these phases are constrained by robust OSL dating and by radiocarbon ages (Briant et al., 2004a, b). Other sites are also OSL dated (Table 1), making this the most comprehensively dated catchment-scale fluvial sequence to date within the gravel-dominated river deposits of lowland Britain.

Following the newly promoted approach of pattern-oriented sampling (Briant et al., 2018), the key characteristics of the sedimentary sequence in the First Terrace gravel have been identified as:

- The development of a fan-like volume of sediments in the area downstream of the limestone escarpment (Fig. 1C).
- The concentration of sedimentation from the early part of the cycle (last interglacial and early last glacial, ca. 130 to 60 ka) in the southern part of the fan, followed by switching of deposition to the northern section in the later parts of the glacial (ca. 60 to 10 ka; Fig. 2). As discussed above, the facies that were deposited during this transitional period (phase 4) had limited sand beds suitable for OSL dating and so this transition is very imprecisely dated.
- A significant hiatus in deposition during the Last Glacial Maximum (LGM), ca. 30-15 ka (Fig. 2, Table 1).

3. Methods

3.1 Model description and justification

CLEOPATRA is a dynamic cellular model driven by an external climate time series. The model enables processes to operate at a grid-cell level (here 100 × 100 m), thus creating opportunities for them to interact in different spatial settings as well as at an aggregate catchment level. It also allows key elements of the landscape to change and be updated with each annual time step rather than being prescribed as initial conditions.

CLEOPATRA was developed specifically to be applied to mid-latitude periglacially affected river catchments such as were common during the last glacial period. Whilst based on the CybErosion model used by Wainwright (2006), CLEOPATRA differs from the CybErosion model in two specific ways, which are described in detail below. First, the vegetation settings have been changed to allow vegetation to grow at lower temperatures. Secondly, the model now explicitly includes periglacial processes, i.e., gelifluxion. The previous configuration of the model only generated precipitation-driven erosion and

therefore had very low sediment delivery at low temperatures. Inclusion of gelifluxion was necessary to adequately replicate a periglacial environment in the model.

The model is dynamic in a number of ways. First, flow routing is not based on a previous specification of the channel location but performed using the D8 routing algorithm that routes all flow in a cell to the steepest downhill neighbour. Secondly, the sediment transport of the model is defined using a travel-distance model, which enables sediment to travel different distances depending on the process by which it was mobilized (see discussion in Wainwright et al., 2008a-c) and avoids the oversimplification of those LEMs that assume all hillslope transfers are diffusive in nature. Third, the vegetation cover is dynamically generated and feeds back into the landscape by changing local evapotranspiration values and therefore reducing the overland flow available to erode the surface. Vegetation in the model grows and dies using a simple logistic growth function, the growth parameter (Eq. 1) which can be either positive or negative as a function of the air temperature (Eq. 2):

$$\frac{dV}{dt} = r^{\pm} V \left(1 - \frac{V}{V_{\max}}\right) \tag{1}$$

where

$$r^{\pm} = \Delta T \left(1 \pm \tanh\left[\frac{T - \tau_*}{\tau_s}\right]\right) \tag{2}$$

These growth functions are limited by a 6°C threshold (τ_*) below which vegetation growth will begin to die off (2). Two scenarios are used in this study: in V', vegetation growth is constrained within a narrow temperature window (τ_s) with an amplitude of 2.5°C above and below the threshold; in V'', vegetation growth and dieback occur over a wider window (τ_s) of 6°C either side of the threshold. The ΔT term represents the change in temperature (°C) compared to the previous year, and the $\pm$ operator has the same sign as ΔT. The total biomass is precipitation-controlled (Wainwright, 2006).

Sediment erosion, transport and deposition by water flow are described in full in Wainwright (2006). Overland flow is calculated based on the permeability of surface material in each cell, itself driven by

the initial parameters for each cell of the depth, stone (>2 mm) and fines (≤2 mm) content of the sediment. The overland flow in the cell is then compared against a threshold which determines how sediment is mobilized from the surface of the cells. Below the threshold surface flow, mobilization is entirely using a diffuse (unconcentrated overland flow) erosion formulation. Above this threshold erosion is split between the unconcentrated and concentrated erosion calculations. The sediment mobilized from these processes is transferred to the cells downslope from the current cell. It is then deposited proportionally based on a simple exponential travel-distance function, which is parameterized and represented separately for the diffuse and concentrated erosion. If the sediment is not all deposited, the remaining sediment is routed to the next downslope cell and the process repeated. The sediment mobilized by the concentrated erosion travels significantly farther than that mobilized by the unconcentrated erosion. The exact proportions are calculated also as a function of the size of the cells used in the model run (in the case of this version the unconcentrated erosion travel coefficient is 0.18 m^{-1} and the concentrated erosion coefficient is 0.042 m^{-1}) to enable appropriate spatial scaling to be represented (see Wainwright et al., 2008a).

As well as water-driven erosion, we also simulate diffuse erosion by periglacial action explicitly, given the known climate of the region during much of the time period simulated. This is different from other diffusion-based slope models that include this only as generic diffusion in the form of the cumulative effects of creep, splash, etc.. Published studies from periglacial environments show multiple processes in operation, from those occurring because of diurnal freezing such as needle ice creep and diurnal frost creep to those that average over the course of a year such as annual frost creep / gelifluxion and plug-like flow (Matsuoka, 2001). Given the annual time step used in this model, we chose to simulate only annual frost creep / gelifluxion associated with seasonal thawing, as it penetrates more deeply and is more geomorphologically effective (Matsuoka, 2001). Neither large-scale mass slope failures nor chemical dissolution nor thermal shock, the latter two of which may be more significant than traditionally thought but have yet to be quantified (Hall, 2013), were included in the model. Large-scale mass slope failures are unlikely given the relatively gentle slopes in the catchment. Calculations show

that gelifluxion operates over a temperature range of mean annual air temperature (MAAT) -20°C ≤ MAAT ≤ 8.75°C. The equation used (3) was that from Culling (1963):

$$Q = -\kappa \frac{\partial z}{\partial x} \quad (3)$$

where Q is sediment flux [m a^{-1}] caused by frost creep/gelifluxion, and κ is the rate coefficient [m a^{-1}] parameterized using the approach of Anderson (2002):

$$\kappa = 0.5\,\beta \sum_{n=1}^{f} \zeta_n^2 \quad (4)$$

where β is strain resulting from ice-lens growth (assumed to lie in the range 0.01-0.03, following Anderson, 2000); f is the number of freeze-thaw events; and ζ is the depth of the freezing event [m].

These equations were parameterized as follows to create a baseline estimation of gelifluxion rate that was used directly in the first three runs and scaled in the later four runs (see below). The number of freeze-thaw events (5) is assumed a second-order polynomial of MAAT based on regression analysis (r^2 = 0.68; p = 2.5 × 10^{-15}) of the data of Grossi et al. (2007):

$$f = 17.011 - 0.1745\,MAAT - 0.0487\,MAAT^2 \quad (5)$$

Depth of the freezing event (6) is also a second-order polynomial of MAAT based on the data of Matsuoka (2001):

$$\zeta = 0.9236 - 0.0601\,MAAT - 0.005\,MAAT^2, \quad (6)$$

although we note that the fit here is much poorer ($r^2 = 0.16$; $p = 0.03$) and thus Eq. (6) should be considered a first-order approximation. In addition, the baseline value of $\beta = 0.02$ was chosen, which is simply the midpoint of Anderson's (2002) range, in the absence of any other information on any dynamic controls on the parameter.

Notably, because this parameterization is based on MAAT, Eqs. (1-4) do not take into account various factors that have been shown to be important in driving processes at the local scale. For example, soil-moisture content / water availability for rock fracture can significantly affect the nature of the relationship between MAAT and cracking rates and depths (Hales and Roering, 2007). In addition, the relationship between MAAT and rock / ground temperature can be affected by rock type, albedo, and aspect (Hall et al., 2005). Nonetheless a significant statistical relationship between MAAT and periglacial soil movement has been observed at a number of sites (Matsuoka, 2001). For these reasons, and given the complexity and added uncertainty involved in estimating the additional parameters that would be required to adjust for rock temperature and water availability on a cell-by-cell basis, we opted for the simpler approach of parameterizing gelifluxion in relation to MAAT only.

At the end of each annual time step the surface of the digital elevation model (DEM) and the sediment-depth data are updated in light of the sediment balance in and out of each cell. Flow routing is thus dynamic within and between separate time steps in the simulation.

3.2. Innovative methods for evaluation

In line with a Pattern-oriented sampling approach (Briant et al., 2018), we have identified above three key characteristics of the geological sequence that we would expect to see reflected in amodel output if the modelling is robust for this specific catchment. To assess the extent to which CLEOPATRA can produce these key characteristics, we have carefully chosen model outputs such as sediment volume, total thickness, and thickness per time step to evaluate the model. We then use time-series data only to explore the relationship between climate and fluvial activity. The spatial and temporal limits of the comparisons were tightly defined to ensure the greatest possible confidence in them (e.g., Fig. 3).

In relation to sediment volume and total thickness, surface change maps are often used to compare broad patterns of modelled and observed sediment deposition. However, the large scale of these comparisons can lead to the overdetection of similarities between the two. To avoid this, we carefully defined the area for volumetric and time-based sediment thickness comparison as the First Terrace fan, in which the bulk of sediments dating from this time period are preserved and across which borehole cross sections have been plotted. This area was spatially defined (Fig. 3). These coordinates were then used in Rockworks (for the original stratigraphic data) and Matlab (for the model output) to calculate the volume of the fan deposits and to draw fence diagrams that are directly comparable with borehole cross sections. For comparison of model output with the two geological sites of Deeping St James and Gibbons (Table 1), coordinates were defined for the edges of each quarried area. Time series were then extracted using Matlab from evenly spaced grid cells falling within these areas.

Temporal definition of phases was also tightly constrained. As discussed above, a number of depositional and erosional phases can be identified during the last glacial cycle in the Welland catchment (Table 1, Fig. 2). The ages of these units were defined as tightly as possible, but the size of the error bars, and the lack of age control on the volumetrically important Phase 4 made an additional timescale also necessary. The additional timescale chosen was Marine Isotope Stages (MIS) from the stacked record of LR04 (Lisiecki and Raymo, 2005). Model data were made comparable with these two schemes by bulking the annual data into predetermined phases, always choosing the younger stage when they were at a boundary. Where geological data was being assigned to MIS, either the most likely stage was used or the sediments were evenly split between stages when they spanned more than one stage. Using MIS allows a common baseline. Whilst it assumes that the fluvial changes are driven by climate, this assumption is not unreasonable, given the climatic changes observed in the fossil records from each sedimentary phase (Table 1; Briant et al., 2004a, b). Use of two schemes allows us to generate comparisons that are more robust, being less dependent on the different limitations of each temporal scheme.

In addition to volumetric comparisons over the whole time period, pattern-based evaluation is also possible using synthetic boreholes. These are a new form of model output that we have developed to enable direct comparison of the patterns in modelled and observed data irrespective of actual volumes

of sediment. A synthetic borehole is generated by converting annual sediment balance data from a time series into an aggregate value for specific time periods, defined either in relation to the known geological sequence or an external constraint, as discussed below. The goodness of fit between synthetic and observed sequences can then be quantified by statistically comparing the thickness of the sediments that fall within each category. Comparison of erosion was not undertaken because this is too poorly constrained chronologically. In this study (see below) gross sediment deposition is different between modelled and observed data, which means that the values, although paired, are not directly comparable. For this reason, we chose Spearman's Rank Correlation Coefficient, which uses only ranked values. To further ensure comparability between the two data types, negative numbers from the modelled runs and zeroes were ranked as equivalent because erosional phases are not preserved in the geological record. The two sites from which synthetic boreholes were generated in this study covered multiple grid cells. Comparison of the multiple time series showed that the pattern and timing of erosion and deposition was the same in all cells, so in each case, a synthetic borehole was only created for the grid cell that produced the largest volume of sediment. This choice was made to maximise the robustness of the comparison by making it clearer which phase (either geological (Table 1) or MIS) was associated with the most sediment deposition. Although this choice biases the model data chosen for evaluation toward the thicker sequences, this is justified because it allows greater differentiation between phases and the patterns seen are similar in all cells.

4. Model setup

4.1. Initial land surface

Because the model runs in this project start at 140,000 years ago, the use of the modern land surface was inappropriate (Temme et al., 2017; Briant et al., 2018). The construction of a palaeoDEM was therefore undertaken, based on what was already known about the broad age and distribution of river sediments in the catchment. Seventy-two boreholes from the British Geological Survey (BGS) were digitized into the geological software Rockworks™ to enable the base of various superficial deposits to be mapped. The 140,000-year palaeoDEM was defined at the base of the First Terrace deposits (Horton

and Downing, 1989; Fig. 1C). The lowest part of the First Terrace sequence is known to contain last interglacial (MIS 5e) deposits (Keen et al., 1999) overlying a thin layer of gravel. Therefore the erosional base of the First Terrace is highly likely to date from the end of the penultimate glacial (MIS 6) – i.e., ca. 140,000 years ago. The palaeoDEM surface was therefore placed beneath the First Terrace and equivalent or younger age deposits (*head* [slope deposits] and Holocene [MIS 1] fen deposits) and at the surface of mapped deposits that were deposited before this time, such as glacial *boulder clay* and sand and gravel, as well as the Second Terrace (an altitudinally higher gravel deposit). This surface defined in the valley bottoms was then merged with the modern surface on the valley sides, using data from the Digimap-based Ordnance Survey 10-m profile (Fig. 1B). Pre-run smoothing during the 500-year spin-up period ensured that a realistic channel network was in place at the start of each model run. Initial sediment thickness was 1 m across all grid cells because test runs (not reported) had shown that changes in sediment thickness had no noticeable effects on model outcomes. The relative percentage of stones and fines at the land surface was estimated based on superficial deposits and bedrock exposed at the surface in BGS mapping of the region (Fig. 1C). Cells falling within each polygon were then assigned relative stone and fine percentages based on various measured sources of particle-size data (Table 2). Note that reported particle-size analysis of soils in England describes the ≤2 mm fraction only.

4.2. Climate data

In contrast with shorter timescale studies (e.g., Coulthard et al., 2005), in this setting no local terrestrial temperature and precipitation record exists that covers the full time period to be modelled, i.e., the last interglacial to the present day. This is a common problem in landscape evolution modelling, which has been mitigated in various ways, for example, removing the climatic component in experimental design (Viveen et al., 2014), estimating runoff variation in relation to global sea level changes (Stange et al., 2016), and using sea surface temperature proxies from adjacent marine records (Geach et al., 2015). In this study, three climate time series were used from a number of more distant climate records. First, the best record for western lowland Europe is the Grande Pile pollen record from the Massif Central in France (Guiot, 1990) that was used to construct the LGP temperature input (Fig. 4). A transfer function

was used by Guiot (1990) to estimate temperature and precipitation values based on past pollen assemblages as recorded in this core, which is theoretically very securely based and has the advantage of providing rainfall and temperature estimates. Temperature estimates were taken directly from these estimates because the modern temperature estimate for the Welland of 9.8ºC (Climate Data, 2015) compares well with between 5 and 10°C from the adjacent plain to 1200 m ASL in the Vosges (closest available climate data: Minářová, 2013). The raw precipitation values estimated from Grande Pile were too high for the Welland, likely because the modern rainfall for Lure, near La Grande Pile, is 887 mm (for 2000-2012; World Weather Online, 2015), noticeably higher than the 588 mm of Welland rainfall (Climate Data, 2015). The ratio of 0.663 (between these modern values) was therefore used to scale the Grande Pile (LGP) precipitation data (Fig. 4A). The main limitation of our LGP climate record is that the Grande Pile data set has gaps because of nondeposition of lake sediments / nonpreservation of pollen at key climatic phases, such as during the LGM, ca. 20,000 years ago. In climate record LGP, linear interpolation was used to fill these gaps. A second record (GPG, Fig. 4B) was created, filling these gaps using scaled trends from the NGRIP record (Andersen et al., 2004). An alternative, more continuous, climate record was also tested (Th). Here, climate data were generated from a North Atlantic Sea Surface Temperature record published by McManus et al. (1999). In addition to greater continuity, this record has the advantage that it enables a more maritime climate to be modelled as a comparison to the continental climate recorded at LGP (Fig. 4B). This record was scaled to a climate data set after Stemerdink et al. (2010). Fig. 4B shows that the Th record contains the most climatic fluctuations and that the main difference between the records is during the LGM / late-glacial periods.

The range of annual temperatures inputted from the climate input data sets were between ca. 9.3°C and ca.-1°C. Local estimates from the Welland catchment based on fossil beetle species assemblages from the older parts of the sequence fall between ca.6 °C and ca.-31°C mean January temperatures and ca. 21°C and ca.7°C mean July temperatures (Keen et al., 1999; Briant, 2002; Briant et al., 2004a, b). These estimates are based on overlapping climate envelopes for species rather than a full statistical transfer function, so they may place undue weight on extreme temperature values, which is especially true for colder temperatures, which beetles might not experience because of the presence of sheltered

microhabitats, but they do provide at least some constraint. Assuming that an annual average is the average of January and July values, the beetle-based estimates give a range of 13.5 to -12.0°C. Whilst this encompasses a wider range of temperatures than the model inputs, especially in the cold periods, the core temperatures from which the beetle reconstructions are most reliable overlap. These estimates are therefore sufficiently similar to those reconstructed from fossil data to be acceptable for running the model.

4.3. Scenarios

Following a 500-year spin-up period, the time series was run at an annual time step for 140,000 years and a grid resolution of 100 m over the 1 656 km^2 catchment. Fourteen runs were undertaken (Table 3). These vary in three main ways: gelifluxion rate, vegetation sensitivity, and the climate time series used. Early test runs (not reported here) suggested that vegetation and gelifluxion were the two most important factors in affecting quantities of sediment generated within the catchment, which is why the scenarios shown here test different values of these. The largest number of runs was undertaken using the LGP time series, where five different gelifluxion rates were assessed: the baseline gelifluxion rate defined above (β = 0.02) and two runs with reduced and increased β values (according to the following scaling values used to multiply the baseline value: SXa = 0.1; SXb = 0.5; SXc = 1; SXd = 1.5; SXe = 3). For each gelifluxion rate, two different vegetation sensitivities were used. For the other two climate timeseries (GPG and Th), only the baseline gelifluxion rate (SXc, β = 0.02) was used, each with two different vegetation sensitivities (Table 3). As shown below, none of these runs generated the thickness of sediment actually seen in the model data. Despite this difference, further runs with yet higher gelifluxion values were not undertaken because they were physically implausible in relation to published values.

5. Results and discussion

5.1. Model evaluation

In relation to the first key catchment characteristic of a fan shape, the surface-change maps (Fig. 5) do often show hotspots of deposition falling within the area defined as First Terrace fan deposits. They also often show a northward extending finger that coincides with an area that is mapped as part of the

First Terrace (Fig. 1C) but not included within the spatially defined area in Fig. 3. Therefore, qualitatively, this first key characteristic is reproduced adequately. However, a quantitative comparison of the volume of sediments observed and simulated (Table 4) shows that even in the run where most sediment is produced, the total sediment volume reached only 41% of the observed volume, with a number of runs producing ca. 20% or less, sometimes even negative volumes. Larger volumes were produced where gelifluxion was higher (i.e., SXe V' LGP and SXe V'' LGP) and climatic variability in the late glacial was higher (i.e., SXc V' GPG and SXc V'' GPG). This volumetric mismatch could be because sediment is remaining in the upland parts of the catchment. The latter explanation seems unlikely from the maps (Fig. 5) as the amounts of deposition in the upland catchment areas and in the northward tongue are never significantly greater than those within the formally defined fan area. Similarly, whilst the fan is likely influenced by initial topography, in that it forms where slope angles decrease as the Welland flows east out of the confined valley within the limestone escarpment, the definition of the palaeoDEM is such that it will have influenced fan formation in the model in the same way as during geological deposition. Alternatively, as discussed in more detail below, the sediment erosion and transport algorithms could either not have fully captured the nature of periglacial processes during the last glacial period or could have transported material beyond the fan area. The observed fan area thins rapidly, suggesting either sediment exhaustion or a rapid decrease in transport rate. The mechanisms that caused these effects are possibly not reflected in the model. A final, highly plausible possibility is that the deposits preserved in the field have been partially sourced from almost *in situ* reworking of a previous thick deposit built up over several glacial-interglacial cycles. Evidence for reworking over multiple cycles comes from the neighbouring catchment of the Nene where deposits spanning MIS 8 to 2 (300–20 ka) all occur within gravels attributed to the First Terrace (Langford et al., 2007). In addition, the presence of patches of till of Anglian (MIS 12, ca. 450 ka) age on the top of hills (Langford and Briant, 2004) shows that there has been significant valley lowering since this time that could have produced sufficient sediment to then be later reworked. This lowering could have occurred either shortly after ice sheet retreat as a result of isostatic adjustment (as seen in rivers and marine records: e.g., Maddy and Bridgland, 2000) or over multiple cycles. The implications of such reworking are discussed in more detail below.

In relation to the second key catchment characteristic — i.e., the concentration of deposition in the southern part of the fan in the early part of the last glacial, switching to the north later — this can be assessed using fence diagrams and synthetic boreholes. Plotting fence diagrams for comparison with observed / interpreted patterns shows this clearly on a large scale (Fig. 6), either using sedimentary phases for comparison or a continuous age scale. The use of fence diagrams also clearly shows the effect of gelifluxion on the amount of sediment generated (Fig. 7) — the fan shape is much less well developed with lower values of the gelifluxion rate coefficient β.

It is possible to quantify the goodness of fit of this observed pattern by increasing the spatial scale to that of a single site using our newly developed synthetic boreholes. The sites chosen were those with the best geochronological constraint: Deeping St James and Gibbons (Table 1). Boreholes were generated from those grid cells with the thickest sequence for each run as described above. At the Gibbons site, Table 5 and Figs 8A and 8B show that very few of the model runs are able to reproduce the patterns in the geological data. The Spearman correlation values are best where gelifluxion rates are either at or just above the baseline (SXc and SXd), particularly for SXd V' LGP. The quality of the fit seems to be independent of whether sedimentary phases or Marine Isotope Stages have been used for temporal constraints. At Deeping St James (Table 5, Figs 9A and 9B), the reproduction of geological data patterns is much worse. Only SXb V' LGP and SXb V'' LGP show a significant correlation with the geological data — and then only when time was defined by phase. This is probably partly a result of assigning sediments to MIS in the absence of tightly constrained geochronology. The greater complexity in the earlier part of the time period, sediments from which are not present at Gibbons, makes it harder to robustly assign sediments to MIS. However, all modelled runs from the representative location at Deeping St James do show more deposition in the earlier part of the last interglacial cycle as expected from the geological data. As two runs show a significant correlation at both sites (SXb V' LGP and SXb V'' LGP – Figs 8 and 9, Table 5), we conclude that the model has performed sufficiently well to be used to explore the links between climate and fluvial activity. However, the lack of a single run that produced excellent correlation for both sites using both methods of constraining time, means that we have chosen to look at three different model run outputs in our discussion below of what evidence exists for climatic control on patterns of erosion and deposition (Fig. 10). These outputs are

chosen as follows: SXe V' LGP, which comes closest to matching the sediment volumes observed in the geological record, despite an insignificant correlation with model data; SXb V' LGP, one of only two runs that show a significant correlation with geological data at Deeping St James; and SXc V' GPG to show the impact of greater climatic variability in inputs (chosen over a run using the Th time series because of more significant correlation at Gibbons).

The third key characteristic observed in the Welland catchment is a hiatus in sedimentation at the Last Glacial Maximum (LGM). This hiatus is suggested very clearly by the large ice-wedge casts at Gibbons and other sites in the northern part of the fan, also by deep cryogenic disturbance features at Maxey and Deeping St James (Fig. 2). It is seen less clearly in the model output. The surface-change maps show some indication of it between 15 and 10 ka (Fig. 5) where the maximum deposition is less than between 30-15 ka and 30-40 ka and much of the fan area shows near-zero deposition, suggesting a period of stability. However, this is later than seen in the geological data, where the hiatus is dated to 30-15 ka. The hiatus is not clear in any of the synthetic boreholes (Figs 8 and 9). Deposition is recorded from this time period from most of the model runs. In many cases it is a little thinner than other time periods but not to the extent observed in the geological record. Possibly this difference arises because the model does not directly represent the freezing of the ground surface and therefore cannot generate complete *landscape shutdown* or *switch off* of sediment transport. Alternatively, this period of widespread ground freezing was relatively short lived within MIS 2. Geochronological constraint is insufficient to determine this and neither can the width of the wedges be used. The ice wedges observed are up to 3 m wide, but the time period over which they developed cannot be quantified because there are too many factors involved in ice-wedge cracking to reliably estimate age from width (Murton and Kolstrup, 2003). The model run that produces the most sediment during the LGM is that using the GPG climate time series, which has significant climatic instability at 20,000 years ago. This result strongly suggests that climatic instability is important in increasing sediment delivery and transport.

Overall however, whilst some elements of the geological record are not fully represented in the model output (the generation of the full volume of fan sediments and the detail of sequences at specific sites), there is a general similarity in the creation of a fan shape and the shift in the locus of deposition from south to north.

5.2. Sediment delivery during nonanalogue periglacial events

Comparison of geological and modelled sediment volumes shows a significant difference between the two. Sediment composition, although important (e.g., Attal, 2017), is not discussed here because of the uncertainty in initial estimates of sediment calibre (Table 2). Two possible explanations may account for this discrepancy. The first relates to the sediment available for transport within the catchment. If this is lower in the model, then low sediment delivery could reflect sediment *starvation* that did not occur in the geological record. Here, this would mean that the larger geological sediment volume reflects reworking of material that was already in the landscape, only some of which was added during the most recent glacial-interglacial cycle. This explanation is plausible because river systems constantly rework sediments within their floodplains and because of the local geology described above. In this scenario, the full depth of the sediments would have been excavated at the start of the glacial period, with addition of material from upslope at each time period, but the bulk of the deposits laid down were sourced from geological *resetting* of older deposits. In this case, the model runs would be showing where the river system was at each time period, and the volume of additional material added. Four cycles of similar sediment delivery to that modelled during the last glacial period would be sufficient to generate the volume of sediment currently recorded within the fan, which was not specified at the start of the model simulation. Four glacial periods (MIS 4-2, 6, 8, and 10) post-date the last time that this catchment was covered with ice during the Anglian (MIS 12, ca. 450 ka; Langford and Briant, 2004) and many of the model runs generate only 25% or less of the recorded sediment volume (Table 4), so this is a plausible explanation. Glacial outwash during the Anglian glaciation might also have introduced some sediment that was then reworked from the landscape. These findings suggest that more thought should be given to using expert evaluation to generate a varying sediment thickness map as an initial input to modelling. Although of necessity, such a map would encounter similar problems to initial DEM specification (Briant et al., 2018). Nonetheless, the possibility of artificially *starving* the modelled system of sediments is sufficiently problematic that this should be considered.

A second explanation for the low modelled rates of sediment delivery is model related, i.e., that sufficient sediment is specified within the catchment but that it is not being mobilised by the model.

During most of the time period, the dominant processes in operation were periglacial. For this reason, the model includes gelifluxion, parameterized with reference to modern processes in periglacial environments, and MAAT. The highest levels of gelifluxion used in the model (β = 0.02 x 3 – SXe) were the highest that seemed physically plausible from the literature, which is why they were not increased further in any model runs. Table 4 and Fig. 7 suggest that the volume of sediment delivered to the fan is strongly tied to the strength of the periglacial processes operating. These processes may be underspecified in the model at present. For example, because the model is annual in formulation, it may underestimate the effects of large magnitude and/or multiple events, which may increase sediment movement considerably. The model also does not include large-scale mass failure events on hillslopes that could deliver a significant amount of sediment to the river system, particularly under the wet conditions that seem likely in the mid-latitudes as discussed below. The rationale for this decision was that the catchment is not sufficiently steep for this mechanism to be a significant producer of sediment. However, a further feature of periglacial systems that is not modelled here is seasonal rather than event-based ground freezing (Matsuoka, 2001), which might increase saturation and the amount of mass movement, even on low angle slopes. No evidence of mass movement deposits were, however, observed in the First Terrace sequence of the Welland (Briant, 2002).

Furthermore, although parameterization must of necessity be based on modern observations, these are not a perfect analogue for last glacial times. Solar radiation in high latitudes has stronger seasonal rhythms than in the mid-latitudes, where diurnal freeze-thaw cycles will be stronger and more frequent. Because sediment delivery is strongly tied to the crossing of such thresholds, gelifluxion rates in periglaciated mid-latitudes may be significantly higher than in high latitudes. However, the effects of these differences on 'the magnitude of ground-surface temperature fluctuations, the downward propagation of resultant temperature waves and consequent rates of ground cooling – … – cannot, as yet, be assessed for the European Pleistocene' (Murton and Kolstrup, 2003, p. 163). These stronger diurnal cycles may also increase the availability of water — a key, but neglected, parameter driving weathering rates in periglacial systems (e.g., Hall, 2013). A further difference between current and last glacial mid-latitude periglacial systems is in the presence or absence of vegetation. Fewer peat deposits

in last glacial deposits compared with their abundance in Arctic permafrost at the present day suggest that vegetation abundance was lower (Murton and Kolstrup, 2003), possibly because of greater land surface instability because of greater climatic instability. If true, this would mean that last glacial land surfaces were more susceptible to frost cracking and erosion for sediment transport. This greater susceptibility to frost cracking might also be evidenced by the presence of ice-wedge casts in Pleistocene gravel deposits when frost cracks do not form in gravel in modern periglacial environments. Conversely, because ground freezing is not explicitly included in CLEOPATRA, times of *landscape shutdown* cannot be modelled and the full variability of sediment delivery could be lost.

Our results therefore support the suggestion that sediment delivery during the last glacial was higher than in present day periglacial environments. Some caution should be exercised however about the scale of this difference because observed sediment volumes may reflect a residue from multiple glacial cycles that were not specified in the initial conditions and because some of the difference is likely attributable to processes that we chose not to parameterize within the model, as discussed above.

5.3. Drivers of incision and aggradation in the Welland during the last glacial

Having evaluated the robustness of the numerical modelling applied, we now assess the effect of climate on sedimentation in the Welland catchment. The seeming coincidence of fossil evidence of climate change in the geological record (Briant et al., 2004a,b) suggests that climate is an important driver of fluvial activity here, but the imprecision of the geological dating does not allow detailed relationships to be observed. Climate is the only external driver parameterised in this experiment, and so any changes seen will be either intrinsic to the catchment or driven by climate. Key climate-related variables often cited in conceptual models are shown in Fig. 10: temperature, precipitation, vegetation (presence controlled by temperature, biomass controlled by precipitation), and gelifluxion (included explicitly in a reduced complexity model for the first time here in CLEOPATRA). For all three climate time series (LGP, GPG, and Th) these four variables have a strong degree of covariance, which is why only LGP is shown. Higher temperatures relate to higher precipitation, higher vegetation and lower gelifluxion. During MIS 4 to 2 (ca. 70 to 25 ka), the relationship between temperature and vegetation breaks down

somewhat because temperatures are too low for vegetation to grow. For those climate time series that include late-glacial fluctuations (e.g., SXc V' GPG; Fig. 10G), a vegetation response can be seen after ca. 20 ka, but it is around half the amplitude of the effects seen in MIS 5. Gelifluxion remains uniformly high throughout MIS 4 to 2, with only a few slight decreases relating to temperature increases.

When discussing climate control, two questions must be addressed: is there evidence of significant extrinsic control by climate and if there is, what is the nature of this? The episodic nature of sediment delivery from hillslope and internal complexity of catchments (slope angles, different sediment storage durations, tributary effects etc.) can all lead to the dominance of intrinsic effects controlling fluvial activity in a catchment (e.g., Attal, 2017; Veldkamp et al., 2017). In the Welland catchment, Fig. 10 shows that climatic control is not the only factor driving the patterns seen. Three sets of model output are shown, which have been chosen as representative of the full set of model runs undertaken (Table 3). SXe V' LGP (Fig. 10E) was chosen because it comes closest to matching the sediment volumes observed in the geological record, despite an insignificant correlation with model data; SXb V' LGP (Fig. 10F) was chosen because it is one of only two runs that show a significant correlation with geological data at both Gibbons and Deeping St James; SXc V' GPG (Fig. 10G) was chosen to show the impact of greater climatic variability in the climate time series. None of these model outputs show any shifts in either incision or aggradation directly linked in time to climatic changes, although Fig. 10G does show short-lived pulses of aggradation at ca. 20 and 15 ka, linked to two rapid climatic fluctuations. Intrinsic effects can be significant even in a reduced-complexity model focussed on climate inputs.

In relation to the nature of climatic control on fluvial activity, many researchers suggest that the majority of the geomorphological work was undertaken at times of transition (e.g., Vandenberghe, 2008), either warm-cold or cold-warm. Maddy (1997) and Bridgland (2000) suggested on the basis of preservation of interglacial deposits at the base of terraces in many British sequences that terrace-forming incision took place at the cold-warm transition. These incision events are typically thought to be mediated by the changing balance between discharge and sediment supply, itself driven by changes in vegetation cover and hydrological regime (Vandenberghe, 2008). Incision and aggradation should be differentiated

within and beyond the normal scope of activity of the river. For example, Gibbard and Lewin (2002) and Lewin and Gibbard (2010) argue that the main phase of bedrock planation took place contemporaneously with deposition, representing a laterally migrating relatively shallow *working depth* of fluvial sediment in a multistorey, multichannel fluvial depositional system in the early part of the glacial stage, no deeper than the ca. 7 m reported from the active Sagavanirktok system in Alaska (Lunt and Bridge, 2004). They suggested that this was followed by a later increase in sediment supply leading to considerable reworking of earlier deposits and some aggradation — these later deposits having higher preservation potential. This pattern is the opposite of the one suggested by the Bridgland and Westaway (2008) model, which suggests early glacial aggradation followed by stability. Both models present a single channel mode of deposition during interglacials, which is at odds with the work of Burrin and Scaife (1984) who suggested that large-scale lowland floodplain deposition during the Holocene actually occurred in a silty braided fluvial system not overlying a gravel base, as suggested in both these models.

Looking at time series of changing cumulative sediment balance over time (Fig. 10) enables us to shed light on the relative importance of climatic transitions or adjustment to climate over a longer time period. Multiple transitions may be important in generating sediment supply. For example, in Table 4, whilst GPG and Th time series have more climate transitions, only runs using GPG show greater sediment volumes than LGP. However, little evidence is present in these model runs for large-scale incision, nor for the dominance of transitional periods in doing geomorphological work. Incision does occur during the last interglacial (centred around ca. 120 ka), but it is gradual and not clearly linked to the abrupt transition shortly after 130 ka that marks the start of this period in the temperature and precipitation records. This gradual nature suggests that the incision occurred as a result of a gradual reduction in sediment supply as a result of very low values of gelifluxion during this time period. Indeed, the whole record appears to be driven by gelifluxion-driven sediment supply. The different fan volumes associated with different values of β (Table 4, Fig. 7) suggest that gelifluxion is a crucial process in supplying sediment to the fan system, and this interpretation is also reflected in Fig. 10. The run with the lowest gelifluxion rate (Fig. 10F, SXb V' LGP) has a negative fan volume over almost the whole of

the climate cycle compared with Figs 10E (SXe V' LGP) and 10F (SXc V' GPG) which reach maximum values of ca. 200 M m^3. However, the model (being annual in formulation) does not represent the changes in hydrological regime that would have occurred at this time. Therefore, modelled discharge variability is artificially low, decreasing the likelihood of rapid incisional events. Following the incision and later fill of the fan as gelifluxion rises at the end of the last interglacial, two further periods occur where gelifluxion rates are lower, around the times of MIS 5.1 and 5.3. In neither are gelifluxion rates as low or prolonged as earlier, so a significant drop in fan height is not seen. However, the pattern is one of either low rates of deposition or gentle degradation of the fan surface. No incision is seen at the transition to MIS 1 in any of the runs using climate time series LGP or Th, despite the dramatic drop in gelifluxion at this time, which may be a result of continued deposition of material already mobilised within the catchment. Where the transition to MIS 1 is marked by greater climatic instability in time series GPG (Fig. 10G), an incision event is observed, followed by rapid infilling associated with gradual warming during the Lateglacial Interstadial and the rapid cooling event of the Younger Dryas. The only other short-lived incision event occurs at ca. 90 ka and only clearly in the run with the highest gelifluxion rates (SXe V' LGP, Fig. 10E), seemingly in response to a rapid decrease in precipitation at a time when vegetation abundance was low and gelifluxion high.

Deposition is also clearly driven by gelifluxion-driven sediment supply (Fig. 10). The only periods where total fan volume is above zero are those where gelifluxion rates are high and vegetation abundances are low (the two being in antiphase because both are driven by temperature values). Deposition begins early in the last glacial, but slowly, dominated by the southern part of the fan until around 85 ka in SXe V' LGP (Fig. 10E) and later (ca. 60 ka) in SXb V' LGP (Fig. 10F) and SXc V' GPG (Fig. 10G). Northern domination of fan deposition occurs from ca. 60 ka in all records. This limited deposition is commensurate with the idea of Lewin and Gibbard (2010) that the early glacial period was one of gradual lateral planation and codeposition of sediments. It is less similar to the significant early aggradation proposed by Bridgland and Westaway (2008). This later aggradation clearly reflects the requirement to generate sufficient sediment from the catchment and the time that it takes for this to occur. If the geological setting of the catchment includes significant thicknesses of

sediment from older glacial cycles, then of course this requirement to generate sediment does not exist, and greater deposition could occur earlier. However, none of the model runs contained such thicknesses of sediment. The long aggradation phase from ca. 60 ka onward represents the bulk of the sediment deposited and coincides with the highest values for gelifluxion in MIS 4 to 2.

Overall, this comparison has shown that deposition and incision are sediment-supply driven and largely controlled by gelifluxion rates. Whilst gelifluxion rates are climatically controlled, the elapsed time has a clear influence, with time needed to build up enough mobile sediment on hillslopes to enable aggradation to happen. This observation suggests that in a sediment-starved scenario, climate change has little impact on the chronology of phases of incision and aggradation. Consequently, the discussion above about whether low sediment delivery in these model runs is a function of sediment starvation because of underspecification of initial sediment on the land surface or low sediment mobilisation because parameterisation does not directly represent nonanalogue mid-latitude periglacial environments becomes critical. Further experiments including thicknesses of preexisting sediments in key areas such as the First Terrace fan could be undertaken to explore this effect further.

6. Conclusions

Numerical modelling can help explain the links between climate and river activity at much higher temporal resolution than the geological record. Robust evaluation against the geological record is, however, a necessary precursor to being able to interpret these results. In this paper we present robustly evaluated model output, using a wide range of tightly spatially and temporally constrained outputs used only for evaluation. We particularly pioneer the quantification of the comparison of synthetic borehole data with geological sequences using Spearman Rank Correlation.

The key conclusions from this study are that:

- The new pattern-oriented sampling approach of Briant et al. (2018) applied here enables much better constrained comparison of model and geological data. Three key catchment characteristics were identified from the geological data, each of which was then evaluated in relation to model data. Volumetric comparisons enabled evaluation of the formation of a First

Terrace *fan* by the model. Directly comparable fence diagrams and our newly developed *synthetic boreholes* allowed the timing and spatial disposition of sediment bodies over time to be evaluated in relation to the second and third key catchment characteristics.

- Sediment deposition within the system was higher than we were able to model using the processes that we chose to include. Some of this difference may reflect reworking of previously emplaced sediment and therefore artificially generated sediment starvation in our model runs because they do not specify this. Some differences are also a result of our choice not to include processes such as frozen ground, mass failure, thermal shock, and subannual hydrological variability, which are likely to be significant but hard to parameterise at present. An intractable amount of difference may also be attributable to the significant difference between present-day and last glacial periglacial environments.

- River activity in this model is driven by sediment supply as a result of changes in gelifluxion variations. Net deposition occurs at times with high gelifluxion rates, presumably driving significant diffuse sediment supply from hillslopes into concentrated erosion and then into the channels. Deposition rates also increased over time, showing the importance of elapsed time and therefore the lack of chronological control of climate on timing of deposition in a sediment-starved scenario. Incision occurs gradually, rather than at exactly the same time as climate transitions, suggesting that it is driven here by sediment supply changes rather than discharge changes. The annual nature of the model means that it does not capture all hydrological regime changes and may therefore underrepresent incision associated with multiple, recurring flood events.

Acknowledgements

Initial modelling for this paper on a different version of the model without periglacial processes (not reported here) was funded by Natural England through the DEFRA Aggregates Levy Sustainability Fund in 2010 (Project TAL 0416) and undertaken by Dr Gareth Mottram. The geological section of this paper

was funded by Newnham College, Cambridge (Mary Anne Ewart Studentship to RMB, 1998-2002). The modelling benefitted from the input of Bob Anderson, Tristram Hales, and Kevin Hall.

References

Andersen, K.K., Azuma, N., Barnola, J.M., Bigler, M., Biscaye, P., Caillon, N., Chappellaz, J., Clausen, H.B., Dahl-Jensen, D., Fischer, H. and Flückiger, J., 2004. High-resolution record of Northern Hemisphere climate extending into the last interglacial period. *Nature*, 431, 147-151.

Anderson, R.S., 2002. Modeling the tor-dotted crests, bedrock edges, and parabolic profiles of high alpine surfaces of the Wind River Range, Wyoming. *Geomorphology* 46, 35-58.

Attal, M., 2017. Linkage between sediment transport and supply in mountain rivers. In: Tsutsumi, D., and Laronne, J.B., eds., *Gravel-Bed Rivers, Processes and Disasters*, Wiley-Blackwell, 329-353.

Blöthe, J.H., Korup, O., 2013. Millennial lag times in the Himalayan sediment routing system. *Earth and Planetary Science Letters* 382, 38-46. DOI:10.1016/j.epsl.2013.08.044.

Blum, M.D. and Törnqvist, T.E., 2000. Fluvial responses to climate and sea-level change: a review and look forward. *Sedimentology* 47, 2-48.

Briant RM. 2002. *Fluvial responses to rapid climate change in eastern England during the last glacial period*. PhD thesis, University of Cambridge.

Briant, R.M., Coope, G.R., Preece, R.C. and Gibbard, P.L. 2004a. The Upper Pleistocene deposits at Deeping St James, Lincolnshire: evidence for Early Devensian fluvial sedimentation. *Quaternaire* 15, 5-15.

Briant, R.M., Coope, G.R., Preece, R.C., Keen, D.H., Boreham, S., Griffiths, H.I., Seddon, M.B. and Gibbard, P.L. 2004b. Fluvial response to Late Devensian aridity, Baston, Lincolnshire, England. *Journal of Quaternary Science*, 19, 479-495.

Briant, R.M., Cohen, K.M., Cordier, S., Demoulin, A., Macklin, M.G., Maddy, D., Mather, A., Rixhon, G., Veldkamp, A., Wainwright, J., Whittaker, A., Wittmann, H. 2018. Pattern oriented field

sampling to enable effective field data-model comparison. *Earth Surface Processes and Landforms* – FACSIMILE Special Issue. doi: 10.1002/esp.4458.

Bridgland, D.R., 2000. River terrace systems in north-west Europe: an archive of environmental change, uplift and early human occupation. *Quaternary Science Reviews* 19, 1293-1303.

Bridgland, D.R. and Westaway, R. 2008. Climatically controlled river terrace staircases: a worldwide Quaternary phenomenon. *Geomorphology* 98, 285-315.

Burrin, P.J. and Scaife, R.G., 1984. Aspects of Holocene valley sedimentation and floodplain development in southern England. *Proceedings of the Geologists' Association*, 95(1), pp.81-96.

Climate Data, 2015. Climate of Market Deeping. Available from: http://en.climate-data.org/location/8629/ [accessed 31/3/15].

Coulthard T.J., Lewin J., Macklin M.G., 2005. Modelling differential catchment response to environmental change. *Geomorphology* 69, 222–241.

Culling, W.E.H., 1963. Soil creep and the development of hillside slopes. *The Journal of Geology* 71, 127-161.

Davey, N.D.W., Bridgland, D.R., Keen, D.H., 1991. Maxey Gravel Pit, near Peterborough (TF1307). In: Lewis, S.G., Whiteman, C.A. & Bridgland, D.R. (Eds) *Central East Anglia and the Fen Basin*. QRA Field Guide, QRA, London, pp.185-208.

Duff, P.Mc.L.D. & Smith, A.J., 1992. *Geology of England and Wales*. The Geological Society, London.

Environment Agency, 2009. *River Basin Management Plan. Anglian River Basin District*. Environment Agency, Bristol. Available online from: publications.environment-agency.gov.uk/PDF/GEAN0910BSPM-E-E.pdf [Accessed 21/2/12].

Environment Agency, 2012. Gauge data for the Welland at Tallington. Available from: http://www.environment-agency.gov.uk/hiflows/station.aspx?31004 [Accessed 21/1/12].

French, C.A.I., 1982. An analysis of the molluscs from an Ipswichian inter-glacial river channel at Maxey, Cambridgeshire, England. *Geological Magazine* 119, 593-598.

Geach, M.R., Viveen, W., Mather, A.E., Telfer, M.W., Fletcher, W.J., Stokes, M., Peyron, O., 2015. An integrated field and numerical modelling study of controls on Late Quaternary fluvial landscape development (Tabernas, southeast Spain). *Earth Surface Processes and Landforms* 40, 1907-1926.

Gibbard, P.L. and Lewin, J. 2002. Climate and related controls on interglacial sedimentation in lowland Britain. *Sedimentary Geology* 151, 187-210.

Grossi, C.M., Brimblecombe, P., Harris, I. 2007. Predicting long-term freeze-thaw risks on Europe built heritage and archaeological sites in a changing climate. *Science of the Total Environment* 377, 273-281.

Guiot, J. 1990. Methodology of the last climatic cycle reconstruction in France from pollen data. *Palaeogeography, Palaeoclimatology, Palaeoecology* 80, 49-69.

Hales, T.C. and Roering, J.J., 2007. Climatic controls on frost cracking and implications for the evolution of bedrock landscapes. *Journal of Geophysical Research* 112, F02033, doi:10.1029/2006JF000616.

Hall, K. 2013. Mechanical Weathering in Cold Regions. In: Pope, G.A. (ed) *Treatise on Geomorphology Volume 4, Weathering and Soils Geomorphology.* San Diego, Academic Press, p.258-276.

Hall, K., Lindgren, B.S., Jackson, P., 2005. Rock albedo and monitoring of thermal conditions in respect of weathering: some expected and some unexpected results. *Earth Surface Processes and Landforms* 30, 801-811.

Horton, A. and Downing, R.A., 1989. *Geology of the Peterborough district* (Vol. 158). HMSO Books.

Hughes, P.D., Gibbard, P.L., Ehlers, J. 2013. Timing of glaciation during the last glacial cycle: evaluating the concept of a global 'Last Glacial Maximum' (LGM). *Earth-Science Reviews* 125, 171–198.

Jerolmack, D.J., Paola, C. 2010. Shredding of environmental signals by sediment transport. *Geophysical Research Letters* 37(19).

Keen, D.H., Bateman, M.D., Coope, G.R., Field, M.H., Langford, H.E., Merry, J.S., Mighall, T.M., 1999 - Sedimentology, palaeoecology and geochronology of Last Interglacial deposits from Deeping St James, Lincolnshire, England. *Journal of Quaternary Science*, 14, 411-436.

Langford, H.E., Briant, R.M., 2004. Post-Anglian Pleistocene deposits of the Peterborough area and the Pleistocene history of the Fen Basin. In: Langford, H.E. and Briant, R.M. (eds). *Nene Valley. Field Guide*, Quaternary Research Association, p.22-35.

Lewin, J and Gibbard, P.L. 2010. Quaternary river terraces in England: forms, sediments and processes. *Geomorphology* 120, 293-311.

Lisiecki, L. E., and Raymo, M. E., 2005. A Pliocene-Pleistocene stack of 57 globally distributed benthic d18O records, *Paleoceanography*, 20, PA1003, doi:10.1029/2004PA001071.

Lunt, I.A. and Bridge, J.S., 2004. Evolution and deposits of a gravelly braid bar and a channel fill, Sagovanirktok River, Alaska. *Sedimentology* 51, 415-432.

Maddy D., 1997. Uplift-driven valley incision and river terrace formation in southern England. *Journal of Quaternary Science* 12, 539-45.

Maddy, D. and Bridgland, D.R., 2000. Accelerated uplift resulting from Anglian glacioisostatic rebound in the Middle Thames Valley, UK?: evidence from the river terrace record. *Quaternary Science Reviews*, 19(16), 1581-1588.

Matsuoka, N. 2001. Solifluction rates, processes and landforms: a global review. *Earth Science Reviews* 55, 107-134.

McManus, J.F., Oppo, D.W., Cullen, J.L., 1999. A 0.5-million-year record of millennial-scale climate variability in the North Atlantic. *Science* 283, 971-975.

Minářová, J. (2013): Climatology of precipitation in the Vosges mountain range area. *AUC Geographica*, 48, No. 2, pp. 51–60

Murton, J.B. and Kolstrup, E., 2003. Ice-wedge casts as indicators of palaeotemperatures: precise proxy or wishful thinking? *Progress in Physical Geography* 27, 155-170.

Pratt-Sitaula, B., Burbank, D.W., Heimsath, A., Ojha, T., 2004. Landscape disequilibrium on 1,000-10,000 year scales, Marsyandi River, Nepal, central Himalaya. *Geomorphology* 58, 223-241. DOI:10.1016/j.geomorph.2003.07.002.

Shanley, K.W. and McCabe, P.J., 1994. Perspectives on the sequence stratigraphy of continental strata. *American Association of Petroleum Geologists Bulletin* 78, 544-568.

Stange K.M., Van Balen R.T., Garcia-Castellanos D., Cloetingh S., 2016. Numerical modelling of Quaternary terrace staircase formation in the Ebro foreland basin, southern Pyrenees, NE Iberia. *Basin Research* 28, 124-146.

Stemerdink C., Maddy D., Bridgland D.R., Veldkamp A., 2010. The construction of a palaeodischarge time series for use in a study of fluvial system development of the Middle to Late Pleistocene Upper Thames. *Journal of Quaternary Science* 25, 447-460.

Temme, A.J.A.M., Armitage, J., Attal, M., van Gorp, W., Coulthard, T.J., Schoorl, J.M., 2017. Developing, choosing and using landscape evolution models to inform field-based landscape reconstruction studies. *Earth Surface Processes and Landforms*, doi: 10.1002/esp.4162.

Turowski, J.M., Badoux, A., Leuzinger, J., Hegglin, R., 2013. Large floods, alluvial overprint, and bedrock erosion. *Earth Surface Processes and Landforms* 38, 947-958. DOI:10.1002/esp.3341.

Van De Wiel, M. J. & Coulthard, T. J., 2010. Self-organized criticality in river basins: Challenging sedimentary records of environmental change. *Geology*. v.38, no. 1, pp. 87–90. doi: 10.1130/G30490.1

Van de Wiel, M. J., Coulthard, T.J., Macklin, M.G. and Lewin, J., 2011. Modelling the response of river systems to environmental change: progress, problems and prospects for palaeo-environmental reconstructions. *Earth-Science Reviews* 104, 167-185. doi: 10.1016/j.earscirev.2010.10.004.

Van Huissteden, Ko (J.), Kasse, C., 2001. Detection of rapid climate change in last glacial fluvial successions in the Netherlands. *Global and Planetary Change* 28, 319-339.

Vandenberghe, J. 2008. The fluvial cycle at cold-warm-cold transitions in lowland regions: a refinement of theory. *Geomorphology* 98, 275-284.

Veldkamp, A., Baartman, J.E.M., Coulthard, T.J., Maddy, D., Schoorl, J.M., Storms, J.E.A., Temme, A.J.A.M., van Balen, R., van De Wiel, M.J., van Gorp, W., Viveen, W., 2017. Two decades of numerical modelling to understand long term fluvial archives: Advances and future perspectives. *Quaternary Science Reviews* 166, 177-187.

Viveen W., Schoorl J.M., Veldkamp A., van Balen R.T., 2014. Modelling the impact of regional uplift and local tectonics on fluvial terrace preservation. *Geomorphology* 210, 119-135.

Wainwright, J., 2006. Degrees of separation: hillslope-channel coupling and the limits of palaeohydrological reconstruction. *Catena* 66, 93–106.

Wainwright, J., Parsons, A.J., Müller, E.N., Brazier, R.E., Powell, D.M., Fenti, B., 2008a. A transport-distance approach to scaling erosion rates: 1. background and model development. *Earth Surface Processes and Landforms* 33, 813–826. DOI: 10.1002/esp.1624.

Wainwright, J., Parsons, A.J., Müller, E.N., Brazier, R.E., Powell, D.M., Fenti, B., 2008b. A transport-distance approach to scaling erosion rates: 2. Sensitivity and evaluation of MAHLERAN. *Earth Surface Processes and Landforms* 33, 962–984. DOI: 10.1002/esp.1623.

Wainwright, J., Parsons, A.J., Müller, E.N., Brazier, R.E., Powell, D.M., Fenti, B., 2008c. A transport-distance approach to scaling erosion rates: 3. Evaluating scaling characteristics of MAHLERAN. *Earth Surface Processes and Landforms* 33, 1113–1128, DOI: 10.1002/esp.1622.

World Weather Online, 2015. Lure Monthly Climate Average, France. http://www.worldweatheronline.com/Lure-weather-averages/Franche-Comte/FR.aspx [Accessed 1st May 2015]

Zar, J.H., 1984. Multiple comparisons. *Biostatistical analysis* 1, 185-205.

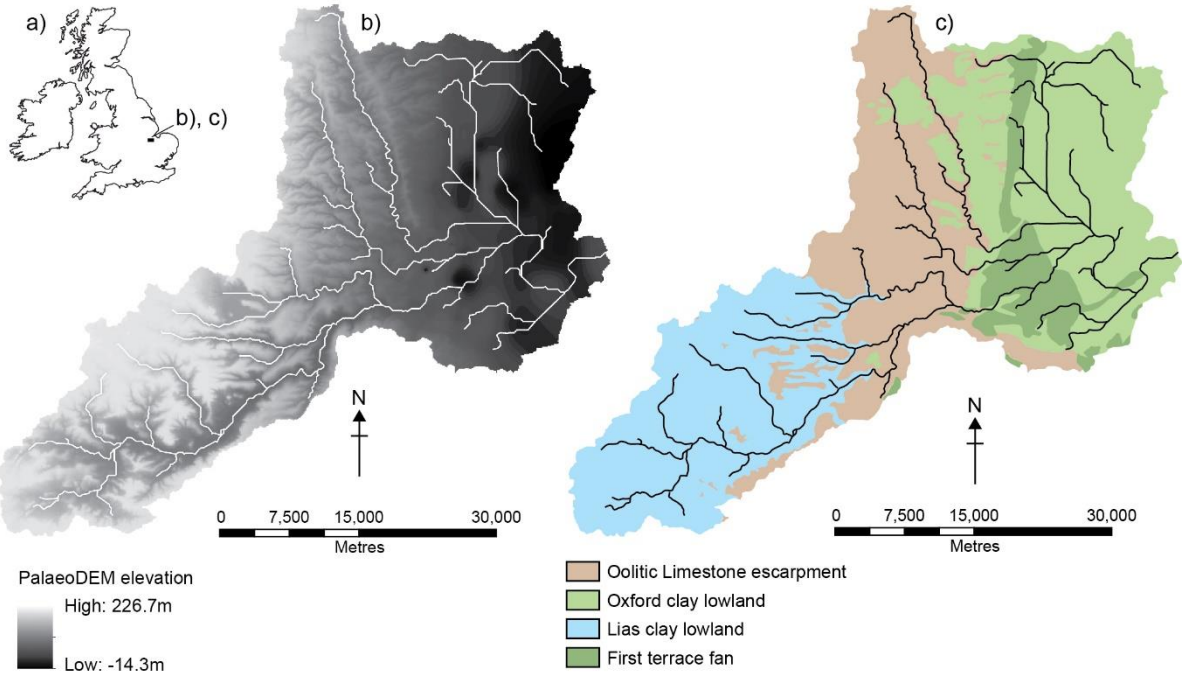

Fig. 1 Location and local geology of the Welland catchment, Lincolnshire, England. (A) Location of catchment within England, (B) topography – palaeoDEM digital elevation model used in full time-length model run. The surface is a combination of the modern surface on the valley sides and the bases of deposits known to have been deposited within this time period on the valley bottoms. Prerun smoothing ensured that a realistic channel network was in place at the start of each model run. The resolution is 100 m. © Crown copyright and database rights 2015. Ordnance Survey [Digimap Licence] (C) key features of bedrock and Quaternary geology and location of sites.

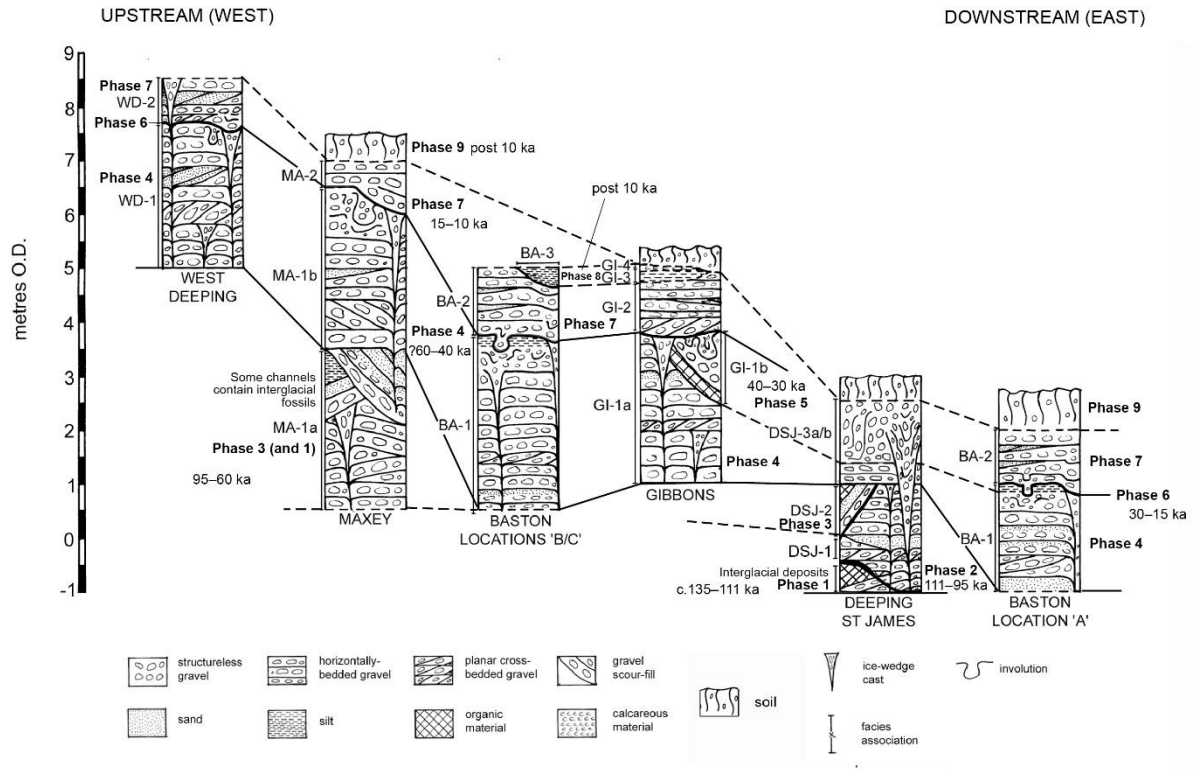

Fig. 2 Summary of the geological sequence from the last glacial-interglacial cycle at six locations in the Welland River catchment (based on French, 1982; Davey et al., 1991; Keen et al., 1999; Briant, 2002; Briant et al., 2004a,b). Details of the interpreted sedimentary phases based on these observations are outlined in Table 1.

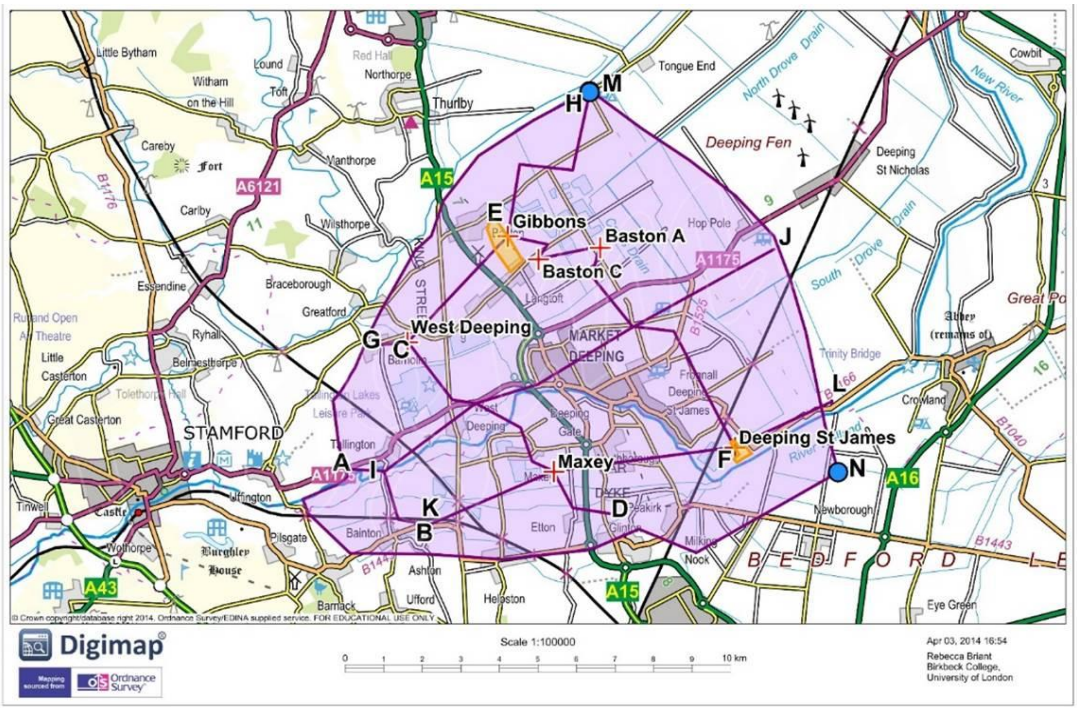

Fig. 3 Map showing the mapped location of the First Terrace fan in purple and transects in the fence diagrams (based on the location of British Geological Survey borehole data and the sites shown in Fig. 2). Line I-J separates the northern and southern halves of the fan.

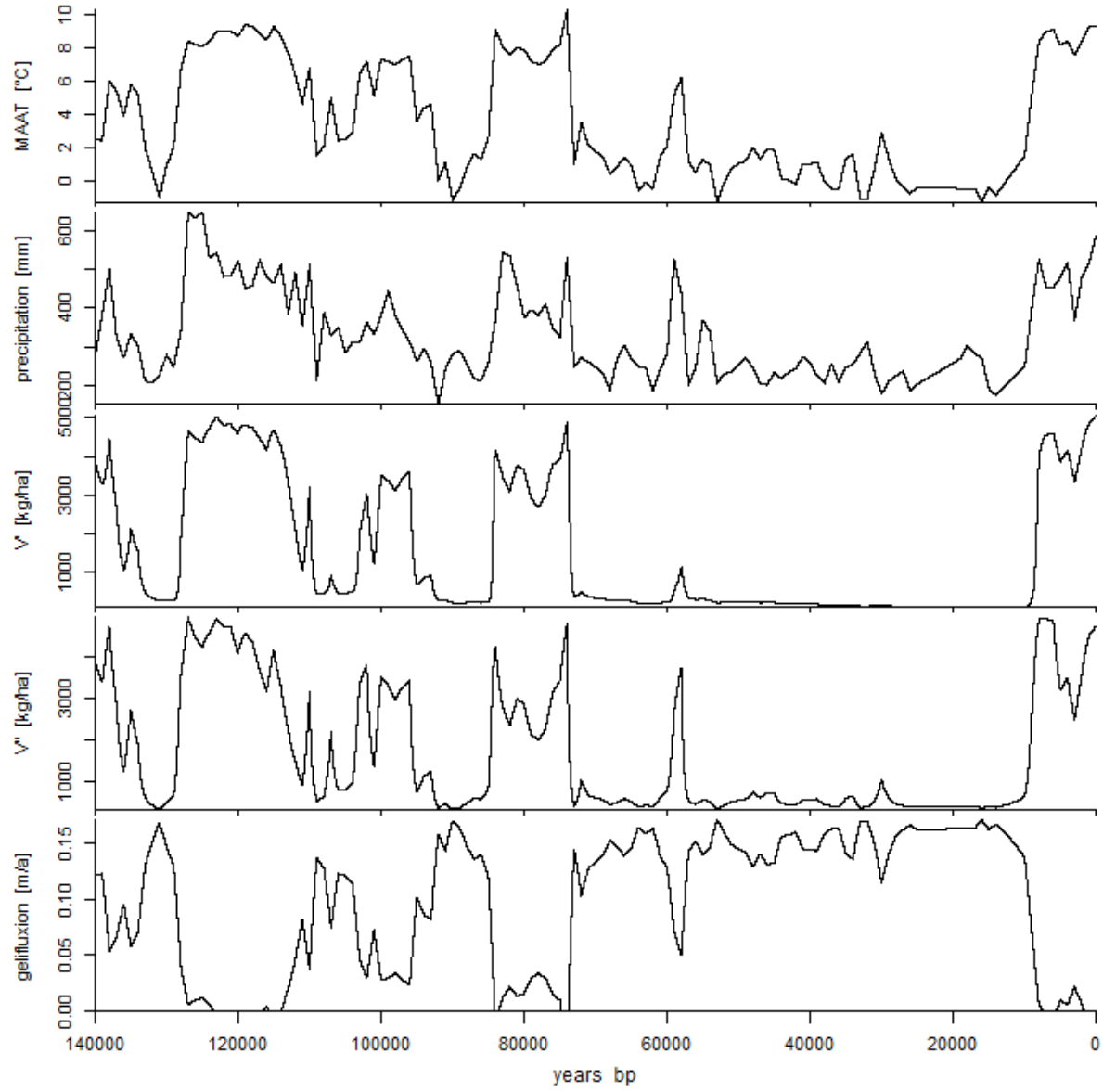
MAAT [°C]
0
2
4
6
8
10
precipitation [mm]
200
400
600
V' [kg/ha]
1000
3000
5000
V'' [kg/ha]
1000
3000
gelifluxion [m/a]
0.00
0.05
0.10
0.15
140000
120000
100000
80000
60000
40000
20000
0
years bp

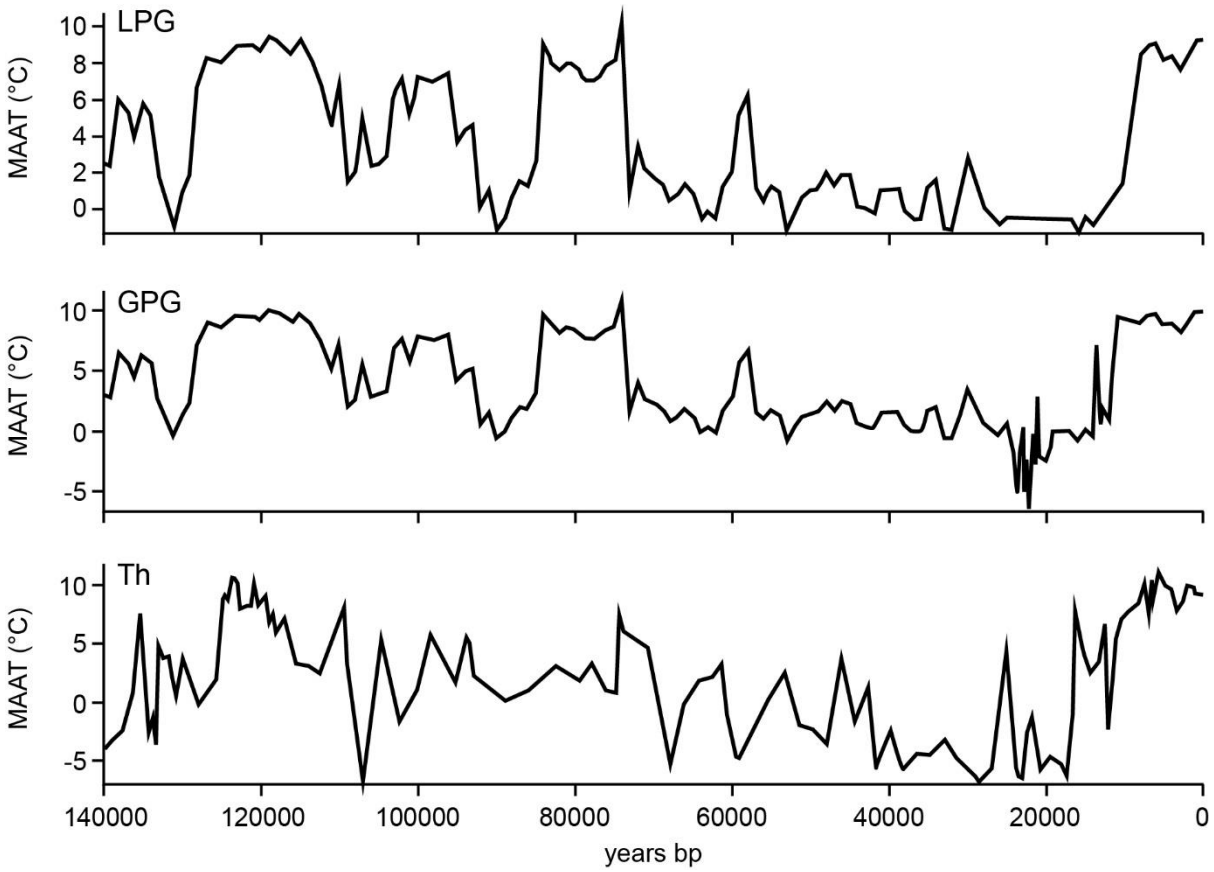

Fig. 4 (A) Precipitation (mm), mean annual air temperature (MAAT, ºC), gelifluction rate coefficient (κ in m a^{-1}), and vegetation response using narrow (V' – 2.5ºC) and wide (V'' – 6ºC) response windows, associated with climate time series LGP – a scaled time series based on temperature reconstructions from La Grande Pile (Guiot, 1990), with linear interpolation through the gaps, for example in the Late-glacial. These variables all scale similarly with all three climate time series. (B) Comparison of the temperature record from LPG with GPG – scaled La Grande Pile (Guiot, 1990) with gaps filled with scaled NGRIP data (Andersen et al., 2004) and Th - scaled North Atlantic SST data (McManus et al., 1999) scaled by Stemerdink et al. (2010) for use in modelling the Thames.

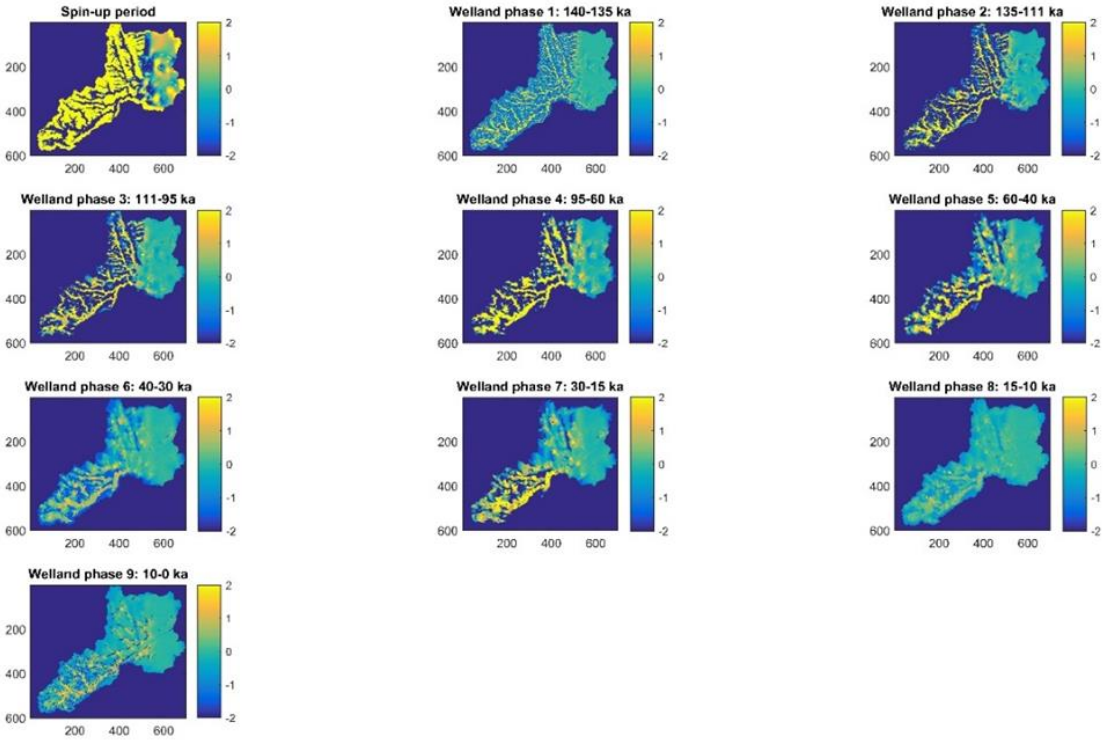

Fig. 5 Surface-change maps from SXc V' LGP, shown as change in elevation between sedimentary phases defined in Table 1. Positive values indicate net aggradation and negative values net erosion. This run was chosen as being the most representative of the patterns seen in all the runs undertaken.

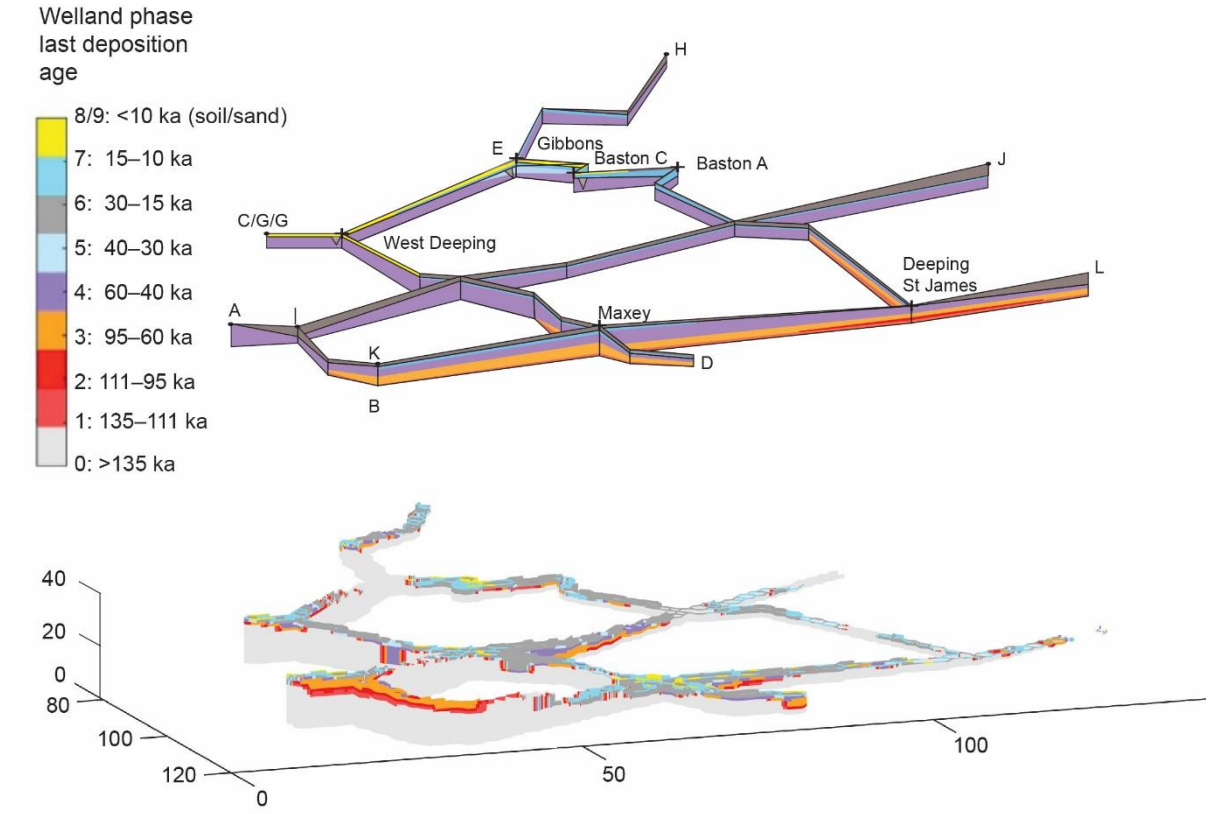

Fig. 6 Fence diagrams showing geological phases of sediment deposition (A), compared with modelled output (B) expressed in the same defined sedimentary phases (Table 2). Run SXc V' GPG (Table 3) is shown as being representative of most model runs.

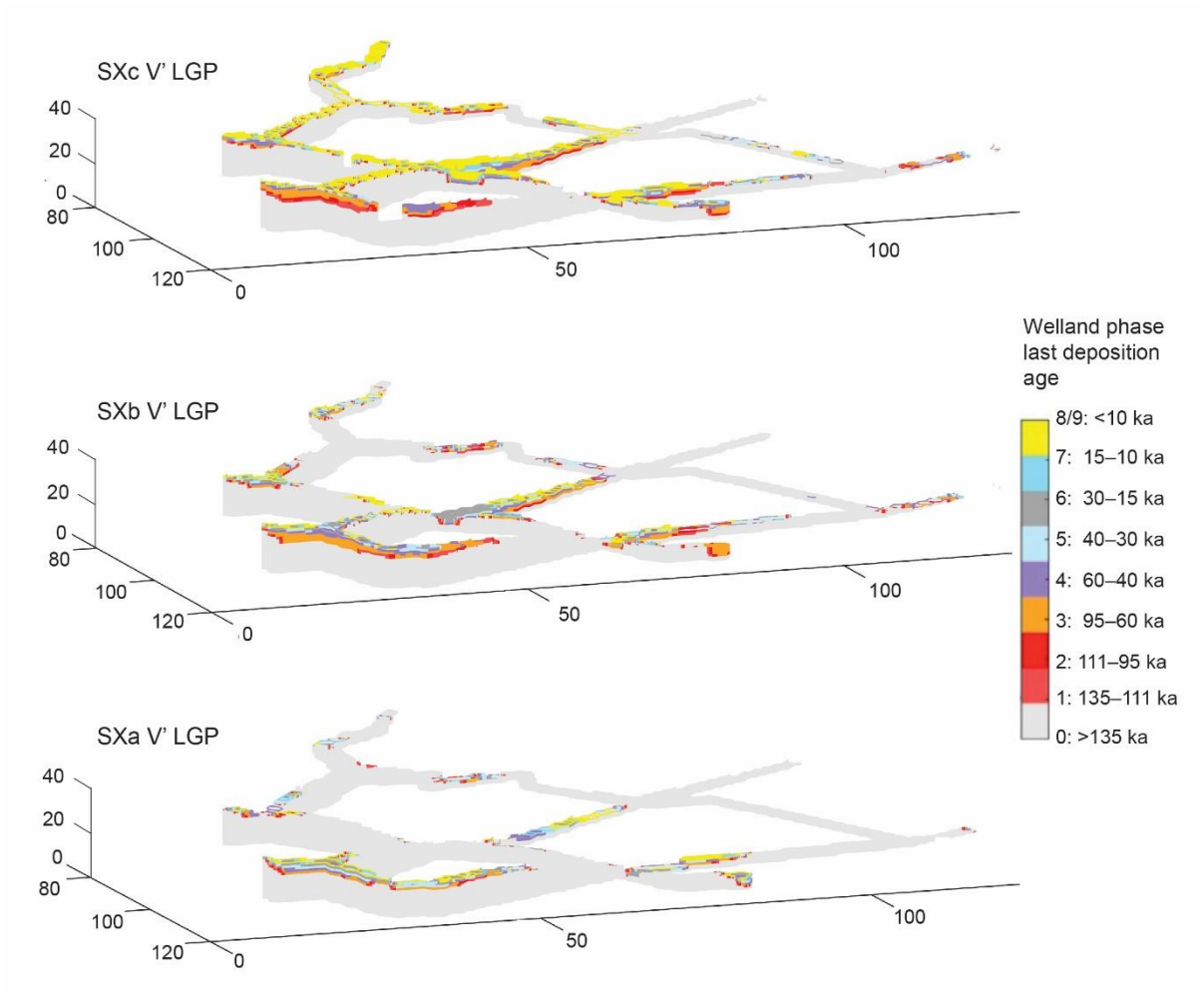

Fig. 7 Fence diagrams showing the difference in development of the fan with a reduction in gelifluxion rate from top to bottom panels (SXc V' LGP, SXb V' LGP, SXa V' LGP – see Table 3 for full details), and thus the importance of gelifluxion in sediment delivery. Outputs from the different modelled runs using SXc were very similar and so a representative example only is shown.

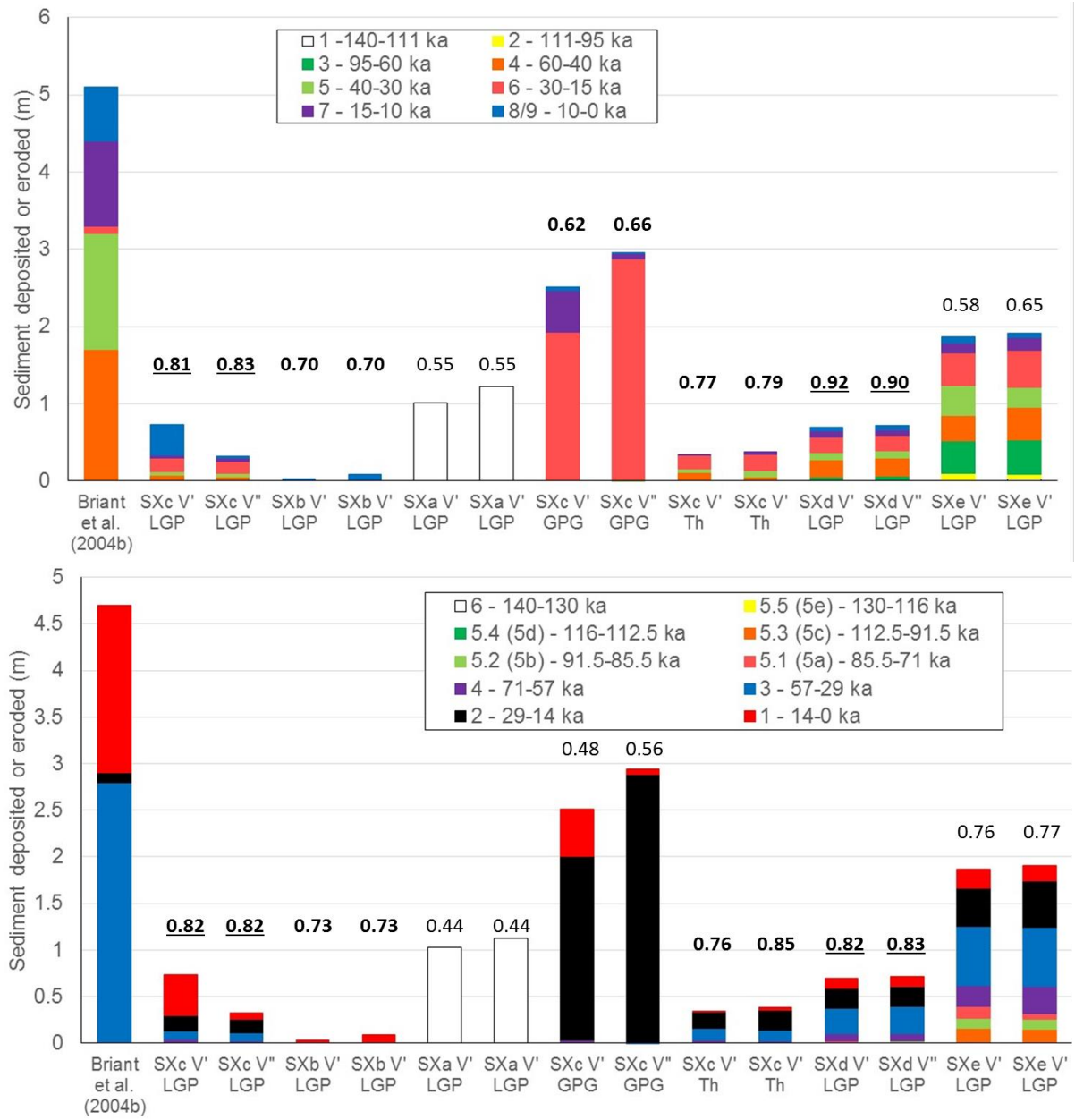

Fig. 8 (A), (B) Comparison of representative *synthetic* boreholes with the observed geology from Gibbon's pit, expressed as both sedimentary phases defined in Table 1 (A) and Marine Isotope Stages from LR04 (Lisiecki and Raymo, 2005) (B). Boreholes chosen were from the grid cells with the thickest sequences within the area coinciding with the quarried deposits, but all grid cells showed the same patterns. Those comparisons which show a significant correlation are highlighted either in bold for 95% significance or bold underlined for 99% significance (as defined in Zar, 1984). N (sample size) was 8 for the Phs time groupings and 10 for the MIS time groupings.

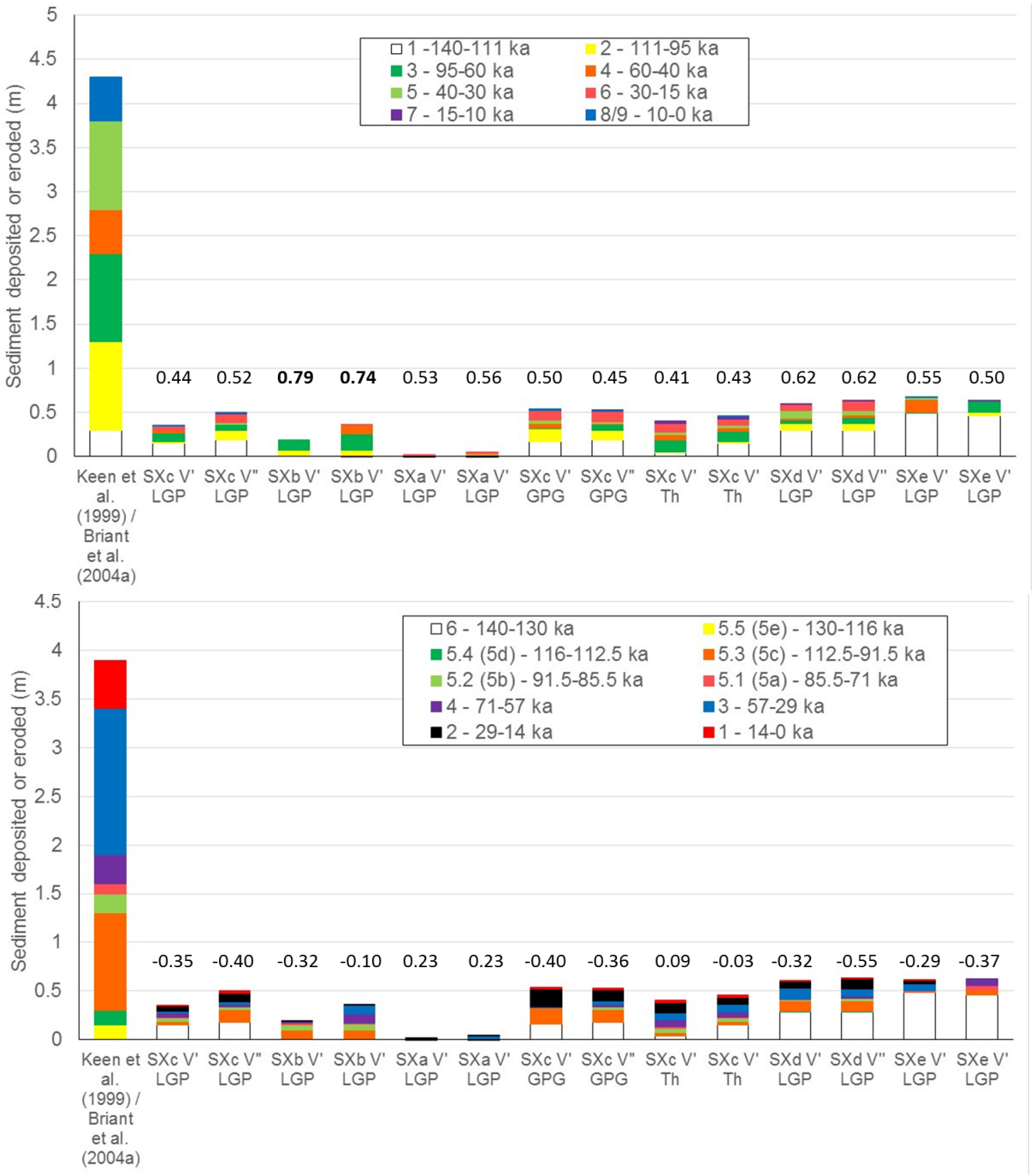

Fig. 9 (A), (B) Comparison of representative *synthetic* boreholes with the observed geology from Deeping St James, expressed as both sedimentary phases defined in Table 1 (A) and Marine Isotope Stages from LR04 (Lisiecki and Raymo, 2005) (B). Boreholes chosen were from the grid cells with the thickest sequences within the area coinciding with the quarried deposits, but all grid cells showed the same patterns. Those comparisons which show a significant correlation are highlighted either in bold for 95% significance or bold underlined for 99% significance (as defined in Zar, 1984). N (sample size) was 8 for the Phs time groupings and 10 for the MIS time groupings.

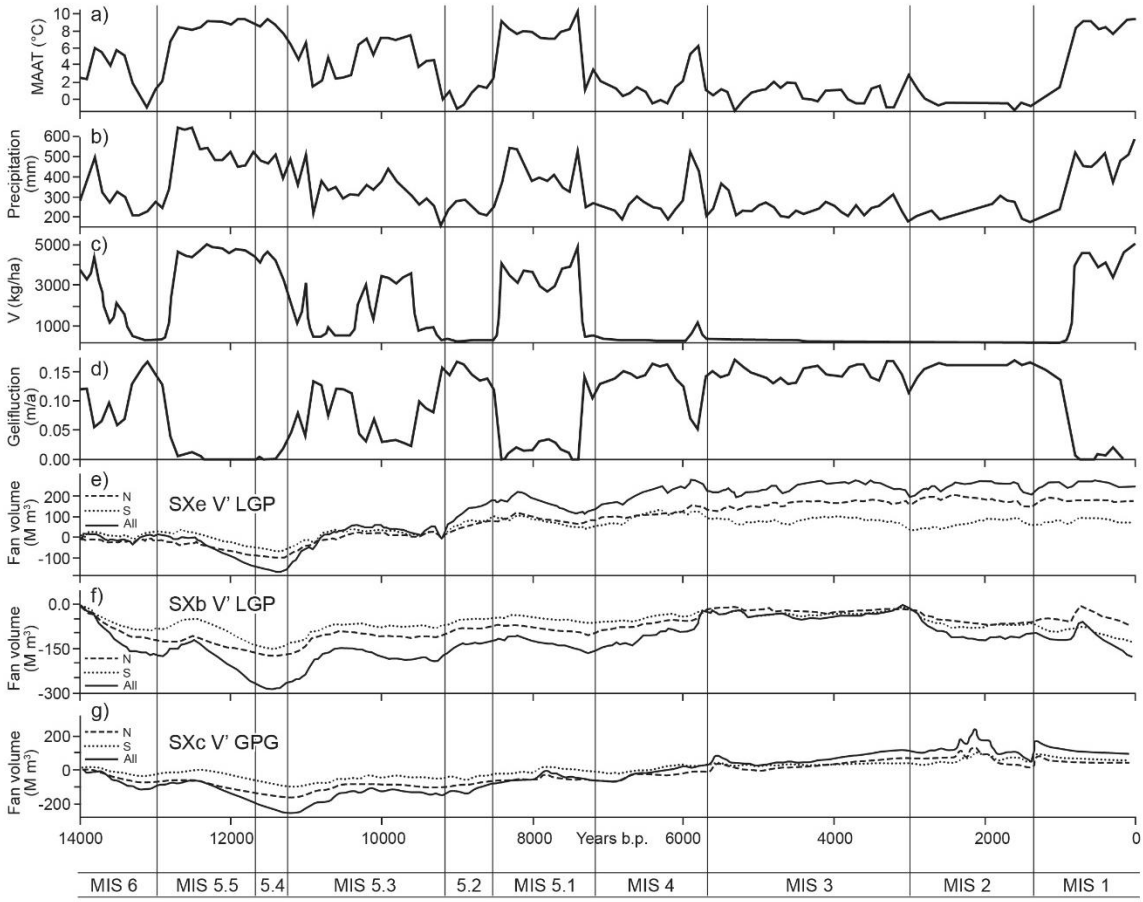

Fig. 10 Time series of (A) temperature data set based on La Grande Pile climate records (LGP); (B) precipitation dataset from La Grande Pile (LGP)cV'; (C) vegetation abundance and (D) rate of gelifluction over time. (E) Shows cumulative sediment balance from SXe V' LGP (chosen because it produced the most sediment – Table 4). (F) Shows cumulative sediment balance from SXb V' LGP (chosen because it showed the best fit to the geological record in the most comparisons - Figs 8A, B; 9A, B). (G) SXc V' GPG (chosen to show the influence of rapid fluctuations in the Late-glacial period). Solid line shows fan volume at a time averaged across the full area of the fan (as defined in Fig. 3, purple area). Dashed line shows the fan volume for the *northern* part of the fan (north of line I-J on Fig. 3). Dotted line shows the fan volume for the 'southern' part of the fan (south of I-J on Fig. 3). Averaging across wider areas reflects the known presence of multiple channels and avoids bias relating to incorrectly assessing the location of the active channel belt.

Table 1

Sedimentological characteristics and interpreted environment of deposition of sediments of successive phases within the Welland catchment, Lincolnshire, England, illustrated in Fig. 2

Sediment phase and estimated time period	**Site and facies assemblage (see Fig. 2)**	**Depositional environment**	**Associated climate events**
9 – post 10 ka	All	Modern soil development	
8 – post 10 ka (based on OSL dating at Baston – Briant, 2002 and Gibbons – Briant et al., 2004b)	Gibbons (GI-4)	Floodplain pool deposition - no longer fluvially active	Holocene – temperate climate
	Baston (BA-3), Gibbons (GI-3)	Aeolian or low-energy fluvial deposition - no longer active	
7 – 15 – 10 ka (based on OSL and radiocarbon dating at Gibbons – Briant et al., 2004b)	Baston (BA-2), Gibbons (GI-2), Maxey (MA-2), West Deeping (WD-2)	Shallow gravel-bed braided river	Late-glacial – peat deposition during the warmer interstadial, fluvial activity during the colder stadial
6 – 30 - 15 ka	Baston, Gibbons, Maxey, West Deeping (Upper surface of BA-1, GI-1, MA-1, WD-1)	Period of widespread ice-wedge development suggesting very low river flows	Last Glacial Maximum
5 – 40 – 30 ka (based on OSL and radiocarbon dating at Gibbons – Briant et al., 2004b)	Gibbons (GI-1b)	Scour-dominated braided river. Possibly lower flows.	MIS 3 – glacial climate
	Deeping St James (DSJ-3b)	Periglacial modification of previously-deposited material - floodplain no longer fluvially active	
4 – 60 - 40 ka (assumed - OSL dating from this unit unreliable – Briant, 2002. Base may be time-transgressive)	Deeping St James (DSJ-3a), Maxey (MA-1b), Baston (BA-1), Gibbons (GI-1a), West Deeping (WD-1)	Shallow gravel-bed braided river, preceded by a period of incision	MIS 4 – 3 – glacial climate
3 – 95 - 60 ka (based on OSL dating at Deeping St James – Briant et al., 2004a)	Deeping St James (DSJ-2), Maxey (MA-1a)	Scour-dominated braided river, preceded by a period of incision at Maxey	MIS 5b – 4 – mostly glacial climates, becoming more severe over time, with one period of lower ice volume in MIS 5a
2 – 111 - 95 ka (based on OSL dating at Deeping St James – Briant et al., 2004a)	Deeping St James (DSJ-1)	Shallow gravel-bed braided river with limited number of active channels, preceded by a period of incision at Deeping St James	MIS 5d (less severe stadial) – MIS 5c (interstadial)
1 – ca. 135 – 111 ka (based on correlation of deposits to the last interglacial)	Deeping St James (Keen et al., 1999), Maxey (French, 1982; Davey et al., 1991)	Low-energy fine-grained deposition during a temperate climate event	Last interglacial / MIS 5e – temperate climate

Further details of individual sites can be found in French (1982), Davey et al. (1991), Keen et al., (1999), Briant (2002), and Briant et al. (2004a,b).

Table 2

Percentage stones and fines values assigned for each of the superficial and bedrock geology types exposed at the surface in the Welland catchment

Lithology	**Stones (>2 mm)**	**Fines (≤2 mm)**	**Data source**
Alluvium	5%	95%	Estimate
Boulder clay	50%	50%	Williams (pers.comm.)
Glacial sand and gravel	70%	30%	Briant (2002)
Marine Gravels	70%	30%	Briant (2002)
River Terrace deposits	70%	30%	Briant (2002)
Cornbrash	20%	80%	Estimate
Great Oolite	20%	80%	Estimate
Inferior Oolite	20%	80%	Estimate
Lower Lias	5%	95%	Estimate
Middle Lias	5%	95%	Estimate
Oxford Clay and Kellaways Beds	0%	100%	Estimate
Triassic mudstones	5%	95%	Estimate
Upper Lias	5%	95%	Estimate

Table 3

Details of modelling runs

Run name	**Initial sediment thickness (m)**	**Gelifluction rate (β value)**	**Vegetation response (V' = narrow range; V'' = wide range)**
SXa V' LGP	1 m	0.02 x 0.1	V'
SXa V'' LGP	1 m	0.02 x 0.1	V''
SXb V' LGP	1 m	0.02 x 0.5	V'
SXb V'' LGP	1 m	0.02 x 0.5	V''
SXc V' LGP	1 m	0.02 x 1	V'
SXc V'' LGP	1 m	0.02 x 1	V''
SXd V' LGP	1 m	0.02 x 1.5	V'
SXd V'' LGP	1 m	0.02 x 1.5	V''
SXe V' LGP	1 m	0.02 x 3	V'
SXe V'' LGP	1 m	0.02 x 3	V''
SXc V' GPG	1 m	0.02 x 1	V'
SXc V'' GPG	1 m	0.02 x 1	V''
SXc V' Th	1 m	0.02 x 1	V'
SXc V'' Th	1 m	0.02 x 1	V''

Table 4

Observed volume of fan sediments compared with modelled volume of fan sediments in the same mapped area.

Source of data	**Volume of sediments within area defined as First Terrace fan in M m^3 of gravel**
Observation (Rockworks)	374
SXa V’ LGP	-33.4
SXa V’’ LGP	-37.9
SXb V’ LGP	9.0
SXb V’’ LGP	12.7
SXc V’ LGP	64.7
SXc V’’ LGP	50.0
SXd V’ LGP	82.2
SXd V’’ LGP	79.9
SXe V’ LGP	157.0
SXe V’’ LGP	154.5
SXc V’ GPG	86.8
SXc V’’ GPG	83.9
SXc V’ Th	59.2
SXc V’’ Th	58.2

Table 5

Results from Spearman rank correlation comparing observed and synthetic sequences at the two key sites of Deeping St James and Gibbons, compared using the two temporal schemes, as shown in Figs 8 and 9

		SXc V' LGP	SXc V'' LGP	SXb V' LGP	SXb V'' LGP	SXa V' LGP	SXa V'' LGP	SXc V' GPG	SXc V'' GPG	SXc V' Th	SXc V'' Th	SXd V' LGP	SXd V'' LGP	SXe V' LGP	SXe V'' LGP
Deeping St James (Keen et al., 1999; Briant et al., 2004a)	Spearman's R - by sedimentary phase	0.44	0.52	**0.79**	**0.74**	0.53	0.56	0.50	0.45	0.41	0.43	0.62	0.62	0.55	0.50
	Spearman's R - by MIS	-0.35	-0.40	-0.32	-0.10	0.23	0.23	-0.40	-0.36	0.09	-0.03	-0.32	-0.55	-0.29	-0.37
		SXc V' LGP	SXc V'' LGP	SXb V' LGP	SXb V'' LGP	SXa V' LGP	SXa V'' LGP	SXc V' GPG	SXc V'' GPG	SXc V' Th	SXc V'' Th	SXd V' LGP	SXd V'' LGP	SXe V' LGP	SXe V'' LGP
Gibbons (Briant et al., 2004b)	Spearman's R - by sedimentary phase	**0.81**	**0.83**	**0.70**	**0.70**	0.55	0.55	**0.62**	**0.66**	**0.77**	**0.79**	**0.92**	**0.90**	0.58	0.65
	Spearman's R - by MIS	**0.82**	**0.82**	**0.73**	**0.73**	0.44	0.44	0.48	0.56	**0.76**	**0.85**	**0.82**	**0.83**	**0.76**	**0.77**

Sedimentary phases (Phs) are defined in Table 2 and Marine Isotope Stages in the stacked marine oxygen isotope record of LR04 (Lisiecki and Raymo, 2005). Negative and zero ranked values were ranked as equivalent to ensure parity between the two types of data. Those comparisons which show a significant correlation are highlighted either in bold for 95% significance or bold underlined for 99% significance (as defined in Zar, 1984). N (sample size) was 8 for the Phs time groupings and 10 for the MIS time groupings.